University of Kent

Kent Academic Repository

Entenberg, David (2018) *Enabling research into the tumour microenvironment: Novel Photonics Assays for Cancer Research.* Doctor of Philosophy (PhD) thesis, University of Kent, None.

Downloaded from

https://kar.kent.ac.uk/70176/ The University of Kent's Academic Repository KAR

The version of record is available from

This document version

UNSPECIFIED

DOI for this version

Licence for this version

CC BY (Attribution)

Additional information

Versions of research works

Versions of Record

If this version is the version of record, it is the same as the published version available on the publisher's web site. Cite as the published version.

Author Accepted Manuscripts

If this document is identified as the Author Accepted Manuscript it is the version after peer review but before type setting, copy editing or publisher branding. Cite as Surname, Initial. (Year) 'Title of article'. To be published in *Title of Journal* , Volume and issue numbers [peer-reviewed accepted version]. Available at: DOI or URL (Accessed: date).

Enquiries

If you have questions about this document contact ResearchSupport@kent.ac.uk. Please include the URL of the record in KAR. If you believe that your, or a third party's rights have been compromised through this document please see our Take Down policy (available from https://www.kent.ac.uk/guides/kar-the-kent-academic-repository#policies).

Enabling research into the tumour microenvironment: Novel Photonics Assays for Cancer Research

by
David Entenberg

Submitted in accordance with the requirements for the degree of Doctor of Philosophy

School of Biosciences
University of Kent
May 2018

Abstract

Physics and engineering principles have long been applied to the development of instrumentation and assays that have significantly advanced biological research. In particular, photonics based instruments and assays have proven to be powerful tools that enable researchers to investigate biological processes in vivo. The research described in this thesis covers a range of photonics based instruments and assays that expand the capabilities researchers have to investigate challenging biological problems. These advances give researchers new tools for directly visualising dynamic biological events in three ways: 1) How to look: novel microscope instrumentation; 2) What to look at: Novel imaging based assays to dissect the tumour microenvironment; and 3) Where to look: Novel surgical protocols to enable ultra-high-resolution optical imaging in living animals (intravital imaging). Application of these assays and instruments to the challenging problem of cancer metastasis has led to a new understanding of the process of intravasation and haematogenous dissemination, paving the way to new clinical diagnostics and therapies.

Word Count: 15,134
Page Count: 78

Acknowledgements

From a very young age, I knew I wanted to be a scientist, and this work is the culmination of that desire. Though my route was indirect, and at times arduous, it has led me to exactly where I want to be, and I could not have wished to be anywhere else.

I have many people to thank for the direction and guidance they have given my life and career, but none so much as my family.

Pamela, who is simply everything; nothing would be possible without her.

Conner and Cavin, in whom I see so much of myself as I had wished to be.

Ian, Debbie, Corinne, Ethan, and Griffin, who have always shown me the good right before my eyes and have given me new optimism for the future.

My mother, taken too early, who taught me to never waste the day or forget to say, “I love you.”

My father who showed me what to demand from life.

My grandparents, whose lives and loves remain a mystery I fear I will never uncover.

Augusta, Milton, Kenneth, and Daniel, a family who instilled in me a respect and passion for learning and exploring.

My mentors John Condeelis, Joan Jones, Maja Oktay, Aviv Bergman, and Ricardo Toledo-Crow: eminent scientists, wonderful teachers, and nurturing colleagues. It is their dedication to science, their patience, and their drive that has allowed me to reach this point. I only hope I can continue to walk in their footsteps.

And finally to Kevin Elicieri whose generosity, encouragement, and example directly led to this work.

Thank you all.

Table of Contents

Abbreviations

2D – Two Dimensional

3D – Three Dimensional

AOTF – Acousto-optic Tuneable Filter

CCD – Charge Coupled Device

CFP – Cyan Fluorescent Protein

EGF – Epidermal Growth Factor

EMCCD – Electron Multiplication Charge Coupled Device

FRET – Forster Resonance Energy Transfer

FPGA – Field Programmable Gate Array

GFP – Green Fluorescent Protein

IVI – Intravital Imaging

LVHR – Large-Volume High-Resolution

NA – Numerical Aperture

NANIVID – Nano Intravital Device

OPO – Optical Parametric Oscillator

ROI – Region of Interest

TIR – Total Internal Reflection

TIRF – Total Internal Reflection Fluorescence

TME – Tumour MicroEnvironemnt

TMEM – Tumour MicroEnvironment of Metastasis

TMEN – Tumour MicroEnvironment Network

WHRIL – Window for High Resolution Imaging of the Lung

Chapter 1: Introduction

Throughout the past century, physics and engineering have played important roles in the development of biological sciences (Botstein, 2010). Advances in instrumentation and the utilisation of concepts from physics have revolutionised the way in which biological research has been conducted (Fields, 2001), and have laid the foundations for the advancement of medicine (Enderle & Bronzino, 2012). In particular, the field of photonics has had a significant impact, with developments such as microscopy and fluorescent biosensors giving researchers the ability to determine the identity, quantity, and location of the cells composing tissues and organs.

Of these, microscopy, through the field of pathology, has defined much of what is known about cells and tissues in health and disease (van den Tweel & Taylor, 2010). However, standard histopathologic analysis requires tissue fixation and sectioning, which limits researchers' ability to study disease processes to a single snapshot in time. Although limited in other ways (small depth of penetration into tissue, requirement for endogeneous or exogenous fluorescent labelling of structures of interest, and necessity of use of anaesthesia) multiphoton imaging in live animals (intravital imaging) removes this restriction by performing optical sectioning in the living tissue, giving the ability to visualise directly the motility and dynamics of cells and tissues in their native environs (Zipfel *et al.*, 2003b).

Mice have been used as experimental models for human diseases for over 100 years (Castle & Little, 1909), and have proven to be an invaluable resource for testing biological theories, principles, and potential therapeutics, especially in the field of cancer research. Through genetic manipulation researchers can create transgenic mice which spontaneously generate tumours that recapitulate the histology of human disease (Lin *et al.*, 2003), or can restrict the native immune system (Bosma *et al.*, 1983), allowing human cancer cell lines and patient derived xenografts to grow at orthotopic locations. This provides a physiologically relevant platform through which the interplay between cancer cells and the host can be examined.

Unfortunately, progress toward a full understanding of the mechanisms underlying metastatic progression, the cause of nearly 90% of all cancer related mortality (Seyfried & Huysentruyt, 2013), has been hampered by the difficulty in applying intravital imaging to study the entire metastatic cascade, including tumour cell dissemination routes, as well as the sites of distant cancer cell colonisation such as the lymphatic system and the lung parenchyma. These internal organs are challenging to access, delicate, and easily damaged. They are also difficult to immobilise which is a crucial requirement for high resolution optical microscopy as motions of just a few microns can blur and distort images.

My research for the past decade has focused on developing enabling technologies for cancer research. The ultimate goal of the research presented in this thesis has been to develop the tools required to study tumour progression and metastasis in the most physiologically relevant manner possible. My work has produced technologies that enable researchers to 1) identify, quantify, and determine the phenotypes of cells within primary and metastatic tumours at single cell resolution, and 2) interrogate the phenotypes of these cells *in vivo* and *in situ*, in both the primary and secondary sites.

To accomplish this, I have employed a unique approach, namely, using engineering principles to develop novel photonics based assays to study cancer progression. These assays fall into three major categories which build toward the ultimate goal of visualising cancer progression and metastatic cascade in living tissues. They are:

1) **Novel microscope instrumentation (How to look)**

Throughout my career, I have utilised my academic training in experimental physics and my industry experience in engineering design to build several instruments and microscopes for cancer research. This includes several microscopes specifically geared toward live cell and

intravital imaging, including: 1) a multi-laser line, total internal reflection fluorescence (TIRF) microscope (Dovas *et al.*, 2011), 2) a multimodal video rate multiphoton / reflectance-confocal microscope (Entenberg *et al.*, 2006) and 3) a two-laser multiphoton microscope capable of exciting fluorophores spanning the entire visible spectrum (Entenberg *et al.*, 2011). As detailed in later chapters, these instruments have been able to directly visualise biological processes such as actin dynamics; differences in metastatic tumour cell motility *in vivo*; intravasation of tumour cells; and arrival, extravasation, and growth of tumour cells in the lung.

2) **Novel imaging based assays to dissect the tumour microenvironment (What to look at)**

Once microscopes and other instruments are in place, developing fluorescently labelled markers for visualising cells and other structures, and their functions, becomes crucial for capturing meaningful information about the biological processes in the tumour microenvironment. At its simplest implementation, fluorescence can be used to label specific cell types by altering the genome of the cells so that they express fluorescent proteins (e.g. green fluorescent protein, or GFP) in their cytosol using cell-type specific promoters. Fluorescent molecules can also be used as biosensors for protein-protein interactions as well as indicators of microenvironmental states such as hypoxia. Therefore, I collaborated with experts in directed evolution and protein design to characterise and utilise fluorescent protein based biosensors that can reveal protein-protein interactions (Förster Resonance Energy Transfer, or FRET, biosensors) (Subach *et al.*, 2012) as well as hypoxic states (hypoxia biosensor) (Wang *et al.*, 2016, Fluegen *et al.*, 2017). Finally, I collaborated with experts in photolithographic engineering to design and develop implantable microfluidic devices capable

of directly altering the immediate environment of living tumours cells (Williams *et al.*, 2016, Fluegen *et al.*, 2017).

3) **Novel surgical protocols to enable ultra-high-resolution optical imaging in living animals: Intravital imaging (Where to look)**

My recent work has focused on expanding the ability to perform high-resolution, single cell intravital imaging of tissues that have not been traditionally imageable intravitally (Harper *et al.*, 2016) and on increasing the utility of the images acquired (Entenberg *et al.*, 2017). My work has enabled visualisation of cellular interactions and processes in the lymphatics (Zolla *et al.*, 2015) and lymph nodes (Das *et al.*, 2013), the untransformed mammary fat pad (Harper *et al.*, 2016), and the lungs (Entenberg *et al.*, 2015, Rodriguez-Tirado *et al.*, 2016).

In summary, my studies have enabled high-resolution imaging of cancer cell dynamics within primary and secondary tumours. In particular, they have revealed the identity (Szulczewski *et al.*, 2016), dynamics (Patsialou *et al.*, 2015), interactions (Patsialou *et al.*, 2013), and biological state (Wang *et al.*, 2016) of tumour cells and their environments and have led to numerous discoveries including identifying the mechanisms underlying intratumoral vascular leakiness associated with cancer cell intravasation (Harney *et al.*, 2015), cancer cell invasion into lymph nodes (Das *et al.*, 2013), and the dynamics of the earliest steps of tumour cell survival and growth in the lungs (Entenberg *et al.*, 2015).

This thesis will be based upon the following publications listed in reverse chronological order. After each reference, my contribution to the work is briefly detailed in italics.

1. **Entenberg D**, Voiculescu S, Guo P, Borriello L, Wang Y, Karagiannis GS, Jones J, Baccay F, Oktay M, Condeelis J. (2017). A permanent window for the murine lung enables high-resolution imaging of cancer metastasis. Nature Methods. PMID: 29176592.

- *Designed and developed an optical imaging window and its accompanying surgical implantation protocol for serial intravital imaging of the murine lung.*

2. **Entenberg D**, Pastoriza JM, Oktay MH, Voiculescu S, Wang Y, Sosa MS, Aguirre-Ghiso J, Condeelis J. (2017). Time-lapsed, large-volume, high-resolution intravital imaging for tissue-wide analysis of single cell dynamics. Methods. 128:65-77. PMID: 28911733 / PMCID: PMC5659295.
    - *Designed and developed surgical protocols for stabilisation of a variety of tissues enabling large-volume high-resolution intravital imaging. Co-wrote the paper.*
3. Sparano JA, Gray R, Oktay MH, **Entenberg D**, Rohan T, Xue X, Donovan M, Peterson M, Shuber A, Hamilton DA, D'Alfonso T, Goldstein LJ, Gertler F, Davidson NE, Condeelis J, Jones J. A metastasis biomarker (MetaSite Breast Score) is associated with distant recurrence in hormone receptor-positive, HER2-negative early-stage breast cancer. NPJ Breast Cancer. 2017;3:42. doi: 10.1038/s41523-017-0043-5. PubMed PMID: 29138761; PMCID: 5678158.
    - *Developed and analytically validated a fully automated digital pathology/image analysis algorithm for the identification and enumeration of a biomarker for metastasis. Evaluated the analytical accuracy, reproducibility, and precision of the test. Co-wrote the paper.*
4. Fluegen G, Avivar-Valderas A, Wang Y, Padgen MR, Williams JK, Nobre AR, Calvo V, Cheung JF, Bravo-Cordero JJ, **Entenberg D**, Castracane J, Verkhusha V, Keely PJ, Condeelis J, Aguirre-Ghiso JA. (2017). Phenotypic heterogeneity of disseminated tumour cells is preset by primary tumour hypoxic microenvironments. Nature Cell Biology. PMID: 28114271.
    - *Designed and developed an implantable device for local induction of hypoxia. Designed photoconversion experiments and co-wrote the paper.*

5. Williams JK, **Entenberg D**, Wang Y, Avivar-Valderas A, Padgen M, Clark A, Aguirre-Ghiso JA, Castracane J, Condeelis JS. (2016). Validation of a device for the active manipulation of the tumour microenvironment during intravital imaging. Intravital. 5(2). PMID: 27790386 / PMCID: PMCPMC5079288. (Co-First Author Publication)
    - *Designed and developed an implantable chemotaxis device for local control of tumour microenvironments during intravital imaging. Co-wrote the paper.*
6. Wang Y, Wang H, Li J, **Entenberg D**, Xue A, Wang W, Condeelis J. (2016). Direct visualization of the phenotype of hypoxic tumour cells at single cell resolution *in vivo* using a new hypoxia probe. Intravital. 5(2). PMID: 27790387 / PMCID: PMCPMC5079291.
    - *Studied hypoxia induced motility differences in in vivo breast cancer models using novel hypoxia probe. Performed intravital imaging and analysed the in vitro and in vivo cell motility data. Co-wrote the paper.*
7. Szulczewski JM, Inman DR, **Entenberg D**, Ponik SM, Aguirre-Ghiso J, Castracane J, Condeelis J, Eliceiri KW, Keely PJ. (2016). *In vivo* Visualization of Stromal Macrophages via label-free FLIM-based metabolite imaging. Scientific Reports. 6:25086. PMID: 27220760 / PMCID: PMCPMC4879594.
    - *Developed techniques for tissue stabilisation utilising breast mammary imaging windows during FLIM imaging.*
8. Rodriguez-Tirado C, Kitamura T, Kato Y, Pollard JW, Condeelis JS, **Entenberg D.** (2016). Long-term High-Resolution Intravital Microscopy in the Lung with a Vacuum Stabilized Imaging Window. Journal of Visualized Experiments. (116):e54603. PMID: 27768066.
    - *Developed experimental protocol, performed all experiments and wrote the paper.*
9. Harper KL, Sosa MS, **Entenberg D**, Hosseini H, Cheung JF, Nobre R, Avivar-Valderas A, Nagi C, Girnius N, Davis RJ, Farias EF, Condeelis J, Klein CA, Aguirre-Ghiso JA.

(2016). Mechanism of early dissemination and metastasis in Her2+ mammary cancer. Nature. PMID: 27974798.

- *Developed a novel intravital imaging protocol for high resolution single cell imaging in the untransformed mammary fat pad. Performed image analysis and three dimensional reconstructions of intravital cell motility movies. Co-wrote the paper.*

10. Harney AS, Wang Y, Condeelis JS, **Entenberg D.** (2016). Extended Time-lapse Intravital Imaging of Real-time Multicellular Dynamics in the Tumour Microenvironment. Journal of Visualized Experiments. (112):e54042. PMID: 27341448 / PMCID: PMCPMC4927790.

    - *Designed protocols to enable long term intravital tumour imaging. Co-wrote the paper.*

11. Zolla V, Nizamutdinova IT, Scharf B, Clement CC, Maejima D, Akl T, Nagai T, Luciani P, Leroux JC, Halin C, Stukes S, Tiwari S, Casadevall A, Jacobs WR, Jr., **Entenberg D**, Zawieja DC, Condeelis J, Fooksman DR, Gashev AA, Santambrogio L. (2015). Aging-related anatomical and biochemical changes in lymphatic collectors impair lymph transport, fluid homeostasis, and pathogen clearance. Aging Cell. 14(4):582-94. PMID: 25982749 / PMCID: PMC4531072.

    - *Developed novel fixturing techniques that enable intravital multiphoton imaging of bacterial flow in mouse hind limb lymphatics.*

12. Patsialou A, Wang Y, Pignatelli J, Chen X, **Entenberg D**, Oktay M, Condeelis JS. (2015). Autocrine CSF1R signaling mediates switching between invasion and proliferation downstream of TGFbeta in claudin-low breast tumour cells. Oncogene. PMID: 25088194 / PMCID: PMC25088194

    - *Performed image analysis and quantification of tumour cell motility. Co-wrote the paper.*

13. Harney AS, Arwert EN, **Entenberg D**, Wang Y, Guo P, Qian BZ, Oktay MH, Pollard JW, Jones JG, Condeelis JS. (2015). Real-Time Imaging Reveals Local, Transient Vascular Permeability, and Tumour Cell Intravasation Stimulated by TIE2hi Macrophage-Derived VEGFA. Cancer Discovery. 5(9):932-43. PMID: 26269515 / PMCID: PMC4560669.
    - *Developed protocols for long term intravital imaging of primary tumours. Developed custom image analysis algorithms of tumour dynamics and performed mathematical modelling of vascular permeability dynamics. Co-wrote the paper.*
14. **Entenberg D**, Rodriguez-Tirado C, Kato Y, Kitamura T, Pollard JW, Condeelis J. (2015). Subcellular resolution optical imaging in the lung reveals early metastatic proliferation and motility. Intravital. 4(3). PMID: 26855844 / PMCID: PMC4737962.
    - *Designed and developed vacuum based lung imaging window and imaging processing algorithms to enable long-term (>12hrs), high resolution, single cell multiphoton imaging. Performed surgery and intravital imaging. Wrote the paper.*
15. Sharma VP, **Entenberg D**, Condeelis J. (2013). High-resolution live-cell imaging and time-lapse microscopy of invadopodium dynamics and tracking analysis. Methods in Molecular Biology. 1046:343-57. PMID: 23868599 / PMCID: PMC3933219.
    - *Designed and developed novel wide-field FRET microscope for high-resolution live-cell imaging. Co-wrote the paper.*
16. Sharma VP, Eddy R, **Entenberg D**, Kai M, Gertler FB, Condeelis J. (2013). Tks5 and SHIP2 regulate invadopodium maturation, but not initiation, in breast carcinoma cells. Current Biology. 23(21):2079-89. PMID: 24206842 / PMCID: PMC3882144.
    - *Developed mechanical designs to incorporate and autofocus module into a FRET microscope, enabling long-term drift-free imaging of single cells. Co-wrote the paper.*

17. Patsialou A, Bravo-Cordero JJ, Wang Y, **Entenberg D**, Liu H, Clarke M, Condeelis JS. (2013). Intravital multiphoton imaging reveals multicellular streaming as a crucial component of *in vivo* cell migration in human breast tumours. Intravital. 2(2):e25294. PMID: 25013744 / PMCID: PMC3908591.
    - *Performed intravital imaging and image analysis of the data to quantify cell motility phenotypes. Co-wrote the paper.*
18. **Entenberg D**, Kedrin D, Wyckoff J, Sahai E, Condeelis J, Segall JE. (2013). Imaging tumour cell movement *in vivo*. Current Protocols in Cell Biology. Chapter 19:Unit19 7. PMID: 23456602 / PMCID: PMC3722061.
    - *Wrote the protocol.*
19. Das S, Sarrou E, Podgrabinska S, Cassella M, Mungamuri SK, Feirt N, Gordon R, Nagi CS, Wang Y, **Entenberg D**, Condeelis J, Skobe M. (2013). Tumour cell entry into the lymph node is controlled by CCL1 chemokine expressed by lymph node lymphatic sinuses. Journal of Experimental Medicine. 210(8):1509-28. PMID: 23878309 / PMCID: PMC3727324.
    - *Performed intravital imaging of metastasis to lymph nodes and performed image analysis of tumour cell motility in the lymphatics and lymph node. Co-wrote the paper.*
20. Subach OM, **Entenberg D**, Condeelis JS, Verkhusha VV. (2012). A FRET-facilitated photoswitching using an orange fluorescent protein with the fast photoconversion kinetics. Journal of the American Chemical Society. 134(36):14789-99. PMID: 22900938 / PMCID: PMC3444247.
    - *Designed experiments to perform 2-photon characterisation of fluorescent proteins. Conceived of the permanence advantage of the construct. Co-wrote the paper.*

21. Hulit J, Kedrin D, Gligorijevic B, **Entenberg D**, Wyckoff J, Condeelis J, Segall JE. (2012). The use of fluorescent proteins for intravital imaging of cancer cell invasion. Methods in Molecular Biology. 872:15-30. PMID: 22700401 / PMCID: PMC4000026.
    - *Wrote section 3.6 of the protocol: Processing Intravital 4D Data*
22. Wyckoff J, Gligorijevic B, **Entenberg D**, Segall J, Condeelis J. (2011). High-resolution multiphoton imaging of tumours *in vivo*. Cold Spring Harb Protocols. 2011(10):1167-84. PMID: 21969629.
    - *Co-wrote the paper.*
23. Wyckoff J, Gligorijevic B, **Entenberg D**, Segall J, Condeelis J. (2011). The *in vivo* invasion assay: preparation and handling of collection needles. Cold Spring Harb Protocols. 2011(10):1232-4. PMID: 21969630.
    - *Co-wrote the paper.*
24. **Entenberg D**, Wyckoff J, Gligorijevic B, Roussos ET, Verkhusha VV, Pollard JW, Condeelis J. (2011). Setup and use of a two-laser multiphoton microscope for multichannel intravital fluorescence imaging. Nature Protocols. 6(10):1500-20. PMID: 21959234.
    - *Designed and developed a novel 2-laser multiphoton microscope system for multi-colour intravital imaging. Designed and developed software for semi-automated analysis of 4D intravital imaging data. Wrote the paper.*
25. Dovas A, Gligorijevic B, Chen X, **Entenberg D**, Condeelis J, Cox D. (2011). Visualization of actin polymerization in invasive structures of macrophages and carcinoma cells using photoconvertible beta-actin-Dendra2 fusion proteins. PloS One. 6(2):e16485. PMID: 21339827 / PMCID: PMC3038862.
    - *Developed novel multi-line automated TIRF microscope. Developed protocol for real time photoconversion of live cells while imaging, enabling live tracking of actin dynamics.*

26. Wyckoff J, Gligorijevic B, **Entenberg D**, Segall JE, Condeelis J. (2010). High-Resolution multiphoton imaging of Tumours *in vivo*. Live Cell Imaging: A Laboratory Manual.441-61. / PMCID: PMC4000043.
    - *Wrote section of chapter on multiphoton microscopy*
27. Gligorijevic B, **Entenberg D**, Kedrin D, Segall J, van Rheenen J, Condeelis J. (2010). Intravital Imaging and Photoswitching in Tumour Invasion and Intravasation Microenvironments. Microscopy Today. 18(1):34-7. PMID: 25635177 / PMCID: PMC4307802.
    - *Co-wrote the paper.*
28. Gligorijevic B, **Entenberg D**, Kedrin D, Segall J, van Rheenen J, Condeelis J. (2009). Intravital imaging and photoswitching in tumour invasion and intravasation microenvironments. Microscopy and Microanalysis. Supplement 2(15):86-7.
    - *Co-wrote the paper.*
29. Dunphy MP, **Entenberg D**, Toledo-Crow R, Larson SM. (2009). *In vivo* microcartography and subcellular imaging of tumour angiogenesis: a novel platform for translational angiogenesis research. Microvascular Research. 78(1):51-6. PMID: 19362098 / PMCID: PMC2739383.
    - *Designed microcartography technique and computational algorithms for relocalisation of regions of interest. Performed intravital imaging. Co-wrote the paper.*
30. **Entenberg D**, Aranda I, Li Y, Toledo-Crow R, Schaer D, Li Y. (2006). Multimodal microscopy of immune cells and melanoma for longitudinal studies. Proceedings of the SPIE. 6081:62-73.
    - *Designed a video rate multiphoton microscope for use with drosophila and cancer research. Co-wrote the paper.*

Chapter 2: Background

The problem

Traditional cancer research has successfully identified the many drivers of cancer initiation: key genes that, when mutated, translocated, or overexpressed, function to either initiate tumour growth (Hanahan & Weinberg, 2011) by improper activation (oncogenes) or by loss of function (tumour suppressor genes). For many years it was thought that the ability to directly target these drivers would significantly improve clinical outcomes (Curtis, 2015). While great improvements in cancer survival have been observed over the past several decades, this has been achieved by many modest reductions in mortality rather than one or a few significant advances (Joy, 2008). The success of cytotoxic chemotherapies and targeted therapies has often been limited by tumour cell escape through therapeutic resistance (Groenendijk & Bernards, 2014, Bergers & Hanahan, 2008), dose limiting on- and off-target toxicities (Gonzalez-Angulo *et al.*, 2007), and dormancy (Aguirre-Ghiso, 2007).

Further, cancer genotyping has not been fully able to identify patients who will eventually develop metastatic disease (Sparano & Solin, 2010). This is of ultimate clinical importance as it has been estimated that about 90% of cancer mortality is due to metastasis (Seyfried & Huysentruyt, 2013). In the absence of this information, many patients whose disease will never progress, and who would be cured by surgery, are over-treated with chemotherapy, while the treatment of others at greatest risk may be stopped prematurely before all systemic disease has been eradicated.

The past decade, however, has been a time of transformation for cancer research in which work such as that of the Tumour MicroEnvironment Network (TMEN) programme at the National Cancer Institute has begun to reveal that tumour initiation and cancer cell dissemination have different driving mechanisms (DeClerck *et al.*, 2017, Swartz *et al.*, 2012). Work within the TMEN revealed that metastatic outcome is determined not only by the genetic mutations that initiate the tumour, but also by the tumour microenvironment: that is, all of the

constituent elements surrounding the tumour cells (e.g. immune cells, extracellular matrix, blood and lymphatic vessels, fibroblasts, etc.) along with their biological state (e.g. hypoxic, stem, proliferating, dormant, etc.).

Thus, a new understanding has emerged about the impact of the tumour microenvironment (TME), and its heterogeneity, upon not just tumour cell proliferation at the primary tumour location, but more importantly, dissemination to, as well as survival, dormancy, and finally re-initiation of growth in secondary sites. A full understanding of this heterogeneity, both temporally and spatially, in the primary and secondary sites, how it supports tumour cell dissemination, dormancy, and eventual further metastatic growth, and how it responds to therapeutic interventions, is crucial since it can reveal commonalities and differences between primary and metastatic sites that could lead to the development of novel therapeutic targets and treatment approaches.

To accomplish this, experiments need to be designed to identify, locate, and characterise the functions and molecular interactions of the cells and structures contributing to the different tumour microenvironments responsible for cancer progression and dissemination. Thus, the best approach is to study tumours and metastases *in vivo*, at widely varying temporal and spatial scales (from minutes to weeks and from sub-cellular to tissue wide) and at different stages of tumour progression (from carcinoma *in situ* on to metastatic growth), in order to give a complete understanding of the biological process. However, only limited progress in understanding metastatic disease has been made using currently available approaches.

While crucial for elucidating the function of genes and proteins of individual cells, conventional tools like 2D *in vitro* assays (Bravo-Cordero *et al.*, 2012) unfortunately do not adequately reflect the complex biology encountered by cells *in vivo* (Bravo-Cordero *et al.*, 2012, Wang *et al.*, 2005). Even 3D *in vitro* assays (Lobov *et al.*, 2007, Noguera-Troise *et al.*, 2006, Goswami *et al.*, 2005), which remove the restrictive topography of 2D assays, still lack the diversity and

heterogeneity of environments present in the living organism (e.g. multiple host cell interactions, physiological extracellular matrix, connection to lymphatic and vascular circuits, etc.). Animal models offer the best opportunity to recapitulate the complex milieu necessary for replication of the clinically relevant tumour microenvironment though they, by virtue of their artificial design (which is necessary for reproducible experimental investigations), still fall short of completely capturing the wide variation of microenvironments observed in the clinic.

One method that has proven extremely useful in elucidating the role that the tumour microenvironment (including hypoxia, epithelial and immune cells, extracellular matrix, stemness, and autocrine/paracrine signalling) has on breast cancer cell dissemination and dormancy *in vivo*, is single-cell resolution multiphoton intravital imaging (IVI) (Entenberg *et al.*, 2011, Wyckoff *et al.*, 2011, Entenberg *et al.*, 2013, Gligorijevic *et al.*, 2010, Gligorijevic *et al.*, 2014, Harney *et al.*, 2015, Giampieri *et al.*, 2009, Masedunskas *et al.*, 2013, Suetsugu *et al.*, 2011, Nakasone *et al.*, 2012, Andresen *et al.*, 2009). Research utilising this technique highlights how high-resolution imaging can identify, localise, and quantify cell types in the tumour microenvironment, *in vivo*, and reveal cell-cell interactions and mechanisms that cannot be observed using fixed tissue. Insights derived from this work on microenvironmental heterogeneity have led directly to practical applications of the information garnered, including new prognostics and companion diagnostics for clinical use (Agarwal *et al.*, 2012, Forse *et al.*, 2015, Rohan *et al.*, 2014).

Novel microscope instrumentation for biological research

Microscopy has been one of the major tools for understanding the biological world (Masters, 2001). In addition to standard wide-field, bright-light microscopy, a number of specialised techniques have been developed that dramatically expand the utility of microscopy by paradoxically placing limitations on how light is utilised. Throughout my career, I have had the opportunity to build several of these microscopes including 1) a multi-channel TIRF microscope (Dovas *et al.*, 2011), 2) a multimodal video rate multiphoton / reflectance-confocal

microscope (Entenberg *et al.*, 2006), and 3) a two-laser multiphoton microscope capable of exciting fluorophores spanning the entire visible spectrum (Entenberg *et al.*, 2011). These microscopes have been utilised to: 1) directly visualise and track the actin cytoskeleton dynamics that lead to the formation of invadopodia and podosomes (subcellular structures cells use to degrade extracellular matrix and migrate through their microenvironment) in tumour cells and macrophages, respectively (Dovas *et al.*, 2011); 2) image tissue response to radiation therapy (Dunphy *et al.*, 2009) and chemotherapy (Karagiannis *et al.*, 2017) *in vivo*; and 3) image tumour cell migration and behaviour *in vivo* (Das *et al.*, 2013, Entenberg *et al.*, 2017, Entenberg *et al.*, 2015, Harney *et al.*, 2015, Harney *et al.*, 2016, Harper *et al.*, 2016, Karagiannis *et al.*, 2017, Patsialou *et al.*, 2013, Patsialou *et al.*, 2015, Wang *et al.*, 2016, Zolla *et al.*, 2015).

The following sections give a general introduction to the theory underlying these microscopy techniques.

Total internal reflection fluorescence (TIRF) microscopy

Wide-field microscopy dramatically increases (by approximately three orders of magnitude) the ability of the human eye to resolve small structures, revealing objects as small as 200 nm (Masters, 2001). However, gaining useful information about proteins and other subcellular structures is often hindered because this resolving power is not isotropic in all three spatial dimensions. Resolution in the direction of the optical axis of the microscope is typically around 5 times as large as in the two perpendicular axes (Richards & Wolf, 1959). This results in the simultaneous collection of light from multiple subcellular structures throughout the sample and leads to a high background and low signal-to-noise ratios. This is demonstrated in **Figure 1A** where tumour cells expressing the fluorescent protein, mCherry, tagged to the cells' endogenous paxillin, can be seen throughout the cell.

In 1956 a method for dramatically reducing this background signal was introduced (Ambrose,

1956) using a microscope setup designed to illuminate the sample at an oblique incidence angle. In this microscope, the sample (a cell suspension in water) was placed on a glass surface and illuminated from within the glass. The trajectory of light traveling in this setup - from a dense material (e.g. glass) into a less dense material (e.g. water) - changes at the interface and, for incidence angles lower than a critical angle, is predicted by Snell's law (which relates the incidence angle to the refracted angle as a function of the speed of light in the two materials). The critical angle is determined as the incidence angle required for the refracted angle to become 90 degrees (i.e. travel parallel to the interface between the two materials). Above this critical angle, all of the energy of the light reflects back into the dense material in a process known as Total Internal Reflection (TIR).

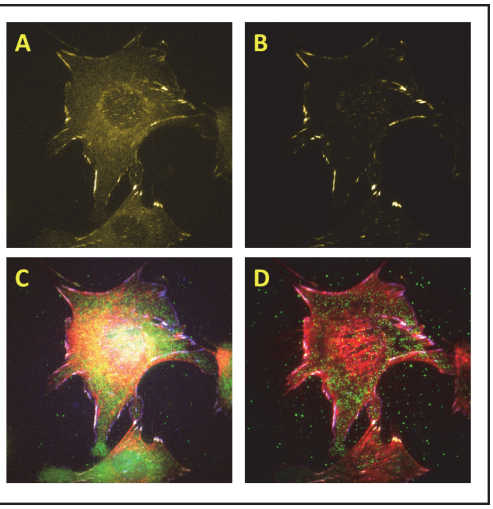

Figure 1: TIRF microscopy can be used to eliminate signal from fluorescently labeled proteins positioned more than ~150 nm from the cover glass-sample interface. A) Epifluorescence microscopy illuminates all molecules within the cell and hence generates a significant amount of background signal. **B)** TIRF microscopy limits the illumination to ~150 nm of the cover glass – sample interface eliminating all fluorescence except for that at the cell's ventral surface, in this case revealing and localizing focal adhesion associated paxillin. **C)** Epi-fluorescence microscopy can visualize several different proteins simultaneously using a combination of immunofluorescence fluorescent proteins **D)** Multi-channel TIRF microscopy allows simultaneous visualization of multiple fluorescent proteins localized to the ventral surface of the cell. **A)-D)** Colors: Blue = Pacific Blue labeled paxillin, Green = Alexa 488 labeled β-actin mRNA, Yellow = mCherry labeled paxillin, Red = phalloidin 660 labeled actin filaments.

While none of the energy of the light in this condition is transmitted into the less dense material, the electric field of the incident wave does however extend slightly beyond the interface boundary as the oscillating light wave is converted into an evanescently decaying field. This exponential decay of the light's electric field occurs over a distance that spans approximately one quarter of the wavelength of the incident light (~100-150 nm). If a material of high density (such as the membrane of a cell) is brought within this decaying field, the field can be converted back to an oscillating wave once again. Thus, the TIR microscope can be used to illuminate only the thin layer of a sample that lies within the evanescent field. All other layers of the sample above this distance remain

unilluminated. **Figure 1B** demonstrates the effect of this directed illumination which reveals only those fluorescently labelled paxillin proteins that are associated with focal adhesions localised on the ventral surface of the cell. However, given the exponential decay of the evanescent field, and its strong dependence upon the indices of refraction of the cover glass and the aqueous media in which the cells reside, determining the exact extent of this thin layer is extremely difficult, if not impossible.

As can be seen in **Figure 1C**, labelling multiple fluorescent proteins simultaneously creates a blurred jumble of signals that makes discerning individual structures exceedingly difficult. My work, presented in Chapter 3 below, centred on designing and developing one of the first multi-channel TIRF microscopes ever to be built, and resulted in a dramatic improvement of isolation and detection of multiple ventral membrane fluorescence signals as can be seen in **Figure 1D**.

Single- and multi-photon fluorescence

At the heart of fluorescence microscopy is the absorption of photons by a material, driving the sample from a lower energy state (typically a ground state) to a higher excited state, followed by the subsequent re-emission of the absorbed energy in the form of light. The efficiency of this light-matter interaction process is dependent both upon the characteristics of the light as well as the matter.

Theories to explain this phenomenon have taken two main forms: the first describes the process in terms of the mechanical motion of a valence electron bound to a nucleus or molecule (Lorentz oscillator model / classical theory) (Boyd, 2008) and the second takes the form of a full quantum mechanical treatment of the atomic/molecular energy states (Goeppert-Mayer model / quantum mechanical theory) (Goppert-Mayer, 2009).

In the classical theory, absorption is understood as a resonance phenomenon wherein the applied electromagnetic waves drive an electron which is bound, in the presence of damping, to a nucleus. The resultant motion of this electron around the nucleus creates a time dependent electric polarisation capable of both absorbing and generating new electromagnetic wave energy. In the simplest case where the binding force is a linear restoring force, the relation between the applied field and the generated polarisation is a linear one ($\boldsymbol{P} = \epsilon_0 \chi^{(1)} \boldsymbol{E}$) (Boyd, 2008), where $\boldsymbol{P}$ is the induced atomic/molecular polarisation, $\boldsymbol{E}$ is the applied electric field, ϵ_0 is the permittivity of free space and $\chi^{(1)}$is the linear electric susceptibility. The resulting equations of motion are thereby also linear and the subsequent generated radiation will be of the same frequency as the driving radiation. The electric susceptibility ($\chi^{(1)}$) in this equation is a direct measure of the strength of the binding force and hence is a function of the matter. In real fluorophores, the presence of a manifold of ground or excited states (vibrational, rotational, etc.) results in a broadened absorption curve. Fast non-radiative decays within these manifolds lead to a spectral separation of the absorption and emission wavelengths (Stokes shift) (Lakowicz, 2006).

When the driving force is large enough to reveal nonlinearities in the binding force, then the equations of motion of the electron will no longer be linear and will no longer be limited to the same frequency as the driving force. The relation between the applied electric field and the generated atomic/molecular polarisation can then be written as a power expansion where the coefficients of the expansion describe the magnitude of nonlinearity of the binding force and resulting strength of each interaction (Boyd, 2008). The imaginary part of the third order electric susceptibility can be used to describe, phenomenologically, the process where two photons are absorbed simultaneously with one photon subsequently re-emitted. If the binding force deviates significantly from a linear force, or if the intensity of the excitation light is strong, then higher order terms in the expansion of the electric susceptibility will be non-negligible,

leading to the simultaneous absorption of three, four, or even more photons. Thus the generic name for these nonlinear interactions between light and matter is “multiphoton absorption”.

While the classical theory is useful in gaining an appreciation and understanding of the non-linear interaction of light and matter, it does not do more than provide a phenomenological description of the mechanism of two photon absorption. For a better, more quantitative understanding of two-photon absorption, a quantum mechanical description is required. Goeppert-Mayer first described the problem in a seminal paper published 1931 where she constructed a framework for the interaction which combines a quantum mechanical description of matter with a classical description of the light field and accounted for interactions between the two with perturbation theory (Goppert-Mayer, 2009).

The key to a conceptual understanding of the interaction is the concept of a virtual state. Eigenfunctions of the molecule are those electron distributions which satisfy the time independent Schrödinger equation. Two such electron distributions, the s and the p orbitals, are shown in **Figure 2A**. While the presence of photons of insufficient energy to bridge the gap between the ground and first excited state cannot cause transitions between these two states, they still interact with the molecule to disturb and temporarily alter the electron distribution.

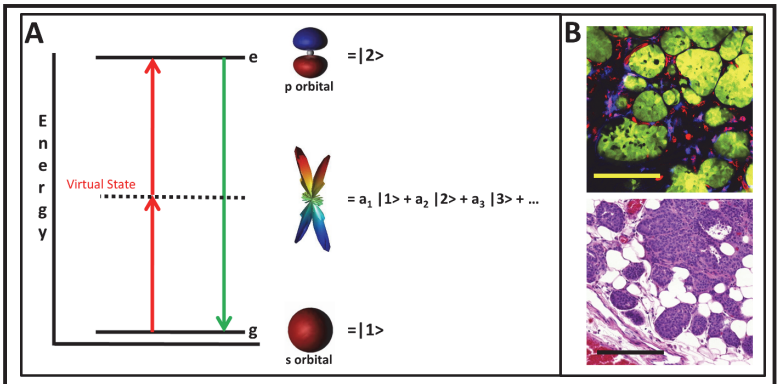

Figure 2: Jablonski energy diagram showing a two-photon absorption process. A) A fluorophore in its ground or excited state has steady-state electron distributions which are solutions to the time independent Schrödinger equation such as an s-orbital (bottom, spherical distribution) or a p-orbital (upper, dumbbell distribution). The presence of a photon of insufficient energy (bottom red arrow) to bridge the ground excited state gap alters this distribution for form a complicated time dependent distribution (middle electron distribution). This distribution, called a “virtual” state, may be described as a coherent superposition of all of the eigenstates of the fluorophore and has an energy equal to the single photon which created it. If a second photon of appropriate energy (upper red arrow) strikes the fluorophore within the lifetime of this time dependent distribution (~10^{-15} s) a transition may occur followed by spontaneous emission of light (green arrow) at twice the frequency of the excitation photons. **B) Top:** Optical section of a spontaneously arising mammary tumour arising in a PyMT-GFP transgenic mouse. Green = tumour cells, blue = second harmonic generation, red = 155kD fluorescently labelled vasculature. Bar = 200 µm. **Bottom:** H&E stained section of the same tumour tissue. Bar = 200 µm.

This is demonstrated by the middle distribution in **Figure 2A**. Since these eigenfunctions form a complete set, this altered state, termed a “virtual” state, with energy midway between the ground and first excited state, may be described by a coherent superposition of the eigenstates (formula next to middle distribution in **Figure 2A**).

While the life-time of these disturbances is very short-lived (~10^{-15} s) (He *et al.*, 2008), if the photon density is high enough, there will be a significant probability that a second photon will strike the distorted distribution within its lifetime and cause a transition. This transition probability, P, is given by (So *et al.*, 2000):

$$P \sim \left| \sum \frac{\langle e | \overrightarrow{\boldsymbol{E_\omega}} \cdot \vec{\boldsymbol{r}} | m \rangle \langle m | \overrightarrow{\boldsymbol{E_\omega}} \cdot \vec{\boldsymbol{r}} | g \rangle}{\varepsilon_\omega - \varepsilon_m} \right|^2$$

Where $|g\rangle$, $|e\rangle$, and $|m\rangle$ are the ground, excited, and middle (perturbed) electron distribution states, $\overrightarrow{\boldsymbol{E_\omega}}$ is the electric field of the excitation light oscillating at a frequency of $\boldsymbol{\omega}$, $\vec{\boldsymbol{r}}$ is the dipole vector of the atom/molecule, $\varepsilon_\omega$is the photonic energy associated with the electric field, and $\varepsilon_m$is the energy difference between the middle state and the ground state.

In practice, photon densities high enough to generate significant multiphoton events are achieved by greatly compressing photons in time and space using a femtosecond pulsed laser focused through a high numerical aperture lens making the technique particularly well suited to microscopy. However, this requirement also limits the ability of the technique to acquire images with low magnification (and hence low numerical aperture) lenses leading to a limited spatial scale, and a loss of context for many samples.

Multiphoton microscopy

The principles of absorption and fluorescence of single photons have been utilised for the addition of contrast to biological samples since the late 1800s with one of the first fluorescence microscopes built in 1910 (Masters, 2010). However, it wasn't until 1990 that the multiphoton process (in particular, two-photon absorption) was applied to laser scanning microscopy (Denk *et al.*, 1990). This combination offers several advantages over standard wide-field, or even confocal, microscopy including: a simpler optical setup and alignment, increased penetration depth, reduced photo-toxicity, reduced photo-bleaching, better contrast in highly absorbing/scattering media, higher sensitivity to weak signals, and better signal-to-noise.

One of the most important of these features is the ability to perform "optical sectioning". As mentioned above, the multiphoton excitation process is greatly enhanced when the photon density is high. In microscopy, this is achieved through the use of a high numerical aperture objective lens which focuses the illumination light to a single point within the sample. Thus, when this point is scanned over a single plane in the sample, excitation only occurs at that single slice. This produces images (**Figure 2B**, top panel) similar to those obtained in histology (**Figure 2B**, bottom panel) where the tissue of interest is chemically treated with preservatives, embedded in wax and physically sliced into sections on the order of five to ten microns. However, instead of this section having been mechanically cut, optical sectioning is non-destructive and the tissue is left intact and alive.

The next chapter is divided into three categories, the first of which details the results of my research beginning with the application of these theoretical principles to the design and construction of novel microscopes. This is followed by the second category which describes the application of these microscopes to the development of novel imaging based assays designed to dissect the tumour microenvironment. The third category describes new techniques aimed at using the instruments and tools developed in category one and two for the study of cancer progression and metastasis *in vivo*. Finally, this work is summed up with

a chapter describing some of the biological discoveries that have been made utilising these novel technologies; discoveries that would not have been possible without these advances.

Category 1: Novel microscope instrumentation (How to look)

A fast-switching, multi-colour total internal reflection fluorescence (TIRF) microscope

In order to build a multichannel TIRF microscope, I utilised a commercially available, single colour TIRF microscope as the base platform. This microscope relied upon off-axis illumination of an extremely high numerical aperture oil immersion objective lens (NA = 1.45) which simultaneously illuminated the sample and collected the generated fluorescence. The optical layout schematic is shown in **Figure 3A**. Here five lasers, spanning the visible spectrum, were combined into a single beam using dichroic mirrors, passed through an acousto-optic tuneable filter (AOTF) - for rapid (~100 ms) and independent intensity and shutter control - and focused into a fibre-optic cable with a fibre coupler. The exit side of the fibre was coupled to a custom designed motorised fibre positioner (**Figure 3B**) driven by a high speed DC servo motor. Computer controlled adjustment of the motor allowed the light exiting the fibre to either travel along the optical axis of the microscope's collimation and tube lenses (resulting in epi illumination of the sample) or be offset from the optical axis, leading to illumination of the sample at a precisely controlled angle. This allows rapid switching between epi- and TIRF illumination, as well as the ability to fine-tune the TIRF angle for each laser line utilised. Incorporation of a deep-cooled, back-illuminated

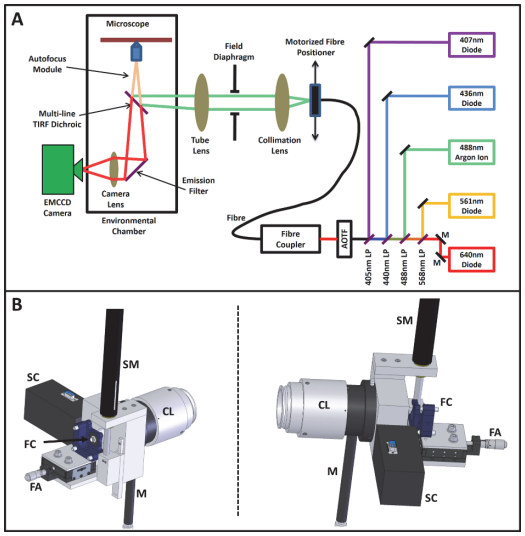

Figure 3: Optical design of the multichannel TIRF microscope. A) Optical layout. 5 laser lines spanning the visible spectrum are combined to a single beam using dichroic mirrors. This beam is passed through an acousto-optic tuneable filter and focused with a fibre coupler into a fibre optic cable. The exit end of the fibre is connected to a motorized fibre positioner. The divergent light is collimated, passed through a field diaphragm and sent on to a tube lens which focuses the beam to the back aperture of a high numerical aperture objective lens. Fluorescence is separated from the illumination light with a multi-line TIRF dichroic and imaged onto an electron multiplication CCD camera. **B)** Computer aided designs showing two different views of the motorized fibre positioner. CL = collimation lens; M = Mount; FA = Fibre Adjuster; SM = Servo Motor; SC = Shutter Controller. Adapted with permission from (Dovas *et al.*, 2011).

electron multiplication CCD (EMCCD) camera allowed collection of extremely low light levels and enabled single molecule detection and tracking.

The system was used to perform direct real-time visualisation of actin cytoskeleton dynamics in tumour cells and macrophages using actin monomers tagged with the photoconvertable fluorescent protein, Dendra2. Use of a genetically encodable fluorescent protein obviated the need to add labelled exogenous monomers and thus avoided the cell permeabilisation artefacts that are associated with such addition.

Using Dendra2-actin, a small soluble population of actin monomers can be converted from green to red resulting in the addition of red monomers to the barbed end of the polymer. The constant green fluorescence allows the visualisation of pre-existing reference filaments onto which polymerisation occurs.

At the same time, unconverted monomers that are removed from the pointed end of the filament will only be green. As a result, fluorescence in the green channel will fluctuate with both polymerisation and depolymerisation of filaments whereas the fluorescence in the red channel will only detect polymerisation.

Photoconversion was achieved by exposing the sample to the UV laser through a nearly fully closed field diaphragm within the illumination arm. This created a circular exposed region (~7 μm in diameter using a 150x objective), which could then be positioned anywhere within the field of view while keeping the rest of the field masked.

Using this technique, we observed that macrophages traffic actin monomers very rapidly (>5 μm/s) from distant parts of the cell to invadopodial precursors and not from local pools, whereas the same process occurs in tumour cells only upon EGF stimulation.

My contribution to this work included: the design and development of the microscope (including design of the mechanics, acquisition electronics, software, and laser beam paths); development of the protocol for photoconversion and acquisition of time-lapse image sequences that revealed the actin cytoskeleton dynamics.

A video-rate multiphoton / reflectance confocal microscope

This microscope, shown in **Figure 4A**, was designed specifically to capture the structure and dynamics of fluorescently labelled neurons in Drosophila larvae (Entenberg D *et al.*, 2004) and immune and melanoma cells in mice (Entenberg *et al.*, 2006). The design of the microscope included several novel features. The first of these was a high-speed, rotating, polygonal mirror that created a point scanning laser system with a pixel dwell time of 115 nanoseconds, resulting in a frame acquisition rate of ~30 frames per second (fps). Rapid switching between objective lenses was accomplished with a custom designed objective holder. A light-tight detection layer containing two non-descanned photomultiplier tubes was closely integrated into the objective holder design to ensure efficient light collection and extraneous light blocking. The 3D computer aided design of the objective holder and collection layer is shown in **Figure 4B**.

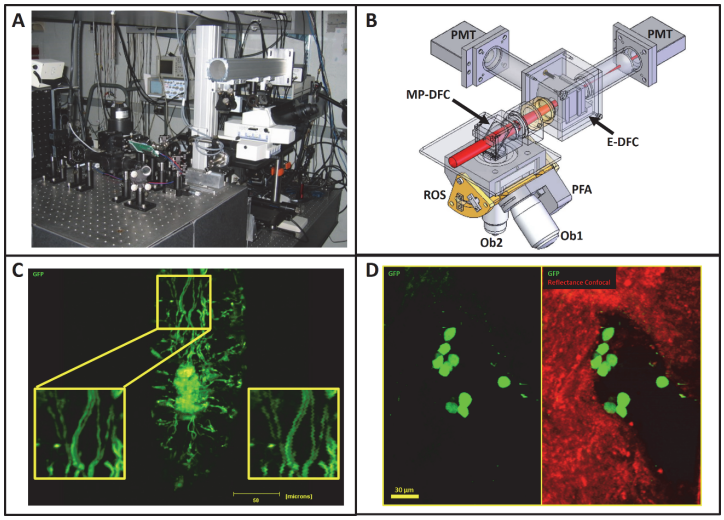

Figure 4: A custom designed, video rate multiphoton/reflectance confocal microscope. A) Photograph of the microscope. **B)** Three dimensional computer aided design of the rapid objective switcher and integrated multiphoton light collection layer for multichannel non-descanned detection. ROS = Rapid Objective Switcher; Ob1 = Objective #1; Ob2 = Objective #2; MP-DFC = Multiphoton Dichroic Filter Cube; E-DFC = Emission Dichroic Filter Cube; PMT = Photomultiplier Tube; PFA = Piezo Focus Adjuster. **C)** Example image of a second instar drosophila larva genetically engineered to express green fluorescent protein in neuronal membranes. **Left inset:** Zoomed in view of neurons. Field of view = 50 µm. **Right inset:** Same field of view as left inset with a simulated two-pixel jitter. **D) Left:** Multiphoton imaging of B16-GFP melanoma cells injected into the epidermis of a mouse lacks context to determine the localization of the tumour cells. **Right:** Addition of a reflectance confocal channel adds the needed context to correctly localize the tumour cells. Here the tumour cells were found to be adherent to the wall of the needle tract (dark hole) through the epidermis. Z-projection of 30 slices taken at a step size of 1 µm per slice.

A separate synchronising laser diode and photodetector independently measured the facet-to-facet error of the rotating polygon and drove the start of the acquisition electronics, reducing the pixel jitter that is endemic to rotating polygons to under 10% of the pixel dwell time. This ensured that fine structures such as neurons, which would most clearly suffer the effects of a pixel jitter, were not distorted. **Figure 4C** shows a drosophila larva whose neurons were transgenically labelled with green fluorescent protein. As can be seen in the left inset image, the neurons are smooth and do not display the zigzag pattern characteristic of pixel jitter as demonstrated in the right inset image which contains a simulated two-pixel jitter.

Finally, backscattered light, which is present in all microscopes, but normally not utilised, was isolated from the incident beam using an optical diode (a half wave plate plus a linear polariser), directed through a 100 μm pinhole, and collected with a high-speed avalanche photodiode. This resulted in a reflectance confocal channel which provided context for cells and tissues that were not otherwise fluorescently labelled. **Figure 4D** demonstrates the importance of this channel in determining the localisation of cells. The left side of **Figure 4D** shows tumour cells that have been injected into the mouse skin. Since multiphoton only generates signal from structures that can be excited by the femtosecond pulsed laser, the cells appear in isolation. Adding in the information captured in the reflected laser beam (red colour in right image) however shows the rest of the epidermis and localises the tumour cells to the inner wall of the needle tract.

The high frame rate of this microscope limits use of slow, but high-gain trans-impedance amplifiers putting the onus of amplification solely on the photo-multiplier tubes (PMTs). For weak fluorescent samples, this can lead to a significant amount of noise imparted upon the signal as PMT are significantly noisier when run at high gain.

My contribution to this work included the design and development of the microscope (including design of the mechanics, acquisition electronics, software, and laser beam path), its construction, and its use in capturing images of fluorescently labelled drosophila larvae and melanoma cells that were injected sub-dermally into mice.

A two-laser multiphoton microscope

Shown in **Figure 5A** is an optical layout, in schematic form, along with a computer aided design drawing of the two-laser multiphoton microscope. **Figure 5B** shows a photograph of the completed system. This microscope was designed specifically for intravital imaging of multiple fluorescently labelled cell types making up the tumour microenvironment in mice (Wyckoff *et al.*, 2011). Excitation of these fluorophores was accomplished by the incorporation of two light sources: a standard titanium-doped sapphire crystal based femtosecond laser, as well as an optical parametric oscillator (OPO) (Entenberg *et al.*, 2011). The former source, a laser capable of output between 700 and 1050 nm can excite fluorophores in the blue, green and orange wavelength ranges. The addition of the OPO as a second light source expands this wavelength range to 1100 to 1600 nm and allows excitation of many red and far-red dyes and fluorescent proteins. As an example, **Figure 5C** shows the two photon brightness and excitation bandwidths for a number of commonly utilised fluorescent proteins taken from the literature (Drobizhev *et al.*, 2007, Drobizhev *et al.*, 2011, Drobizhev *et al.*, 2009, Hoshi *et al.*, 2004, Kawano *et al.*, 2008, Kobat *et al.*, 2009, Kogure *et al.*, 2008, Tillo *et al.*, 2010, Vadakkan *et al.*, 2009, Zipfel *et al.*, 2003a, Nifosì & Tozzini, 2011, Piatkevich *et al.*, 2010) and from the Developmental Resource for Biophysical Imaging Optoelectronics website (http://www.drbio.cornell.edu/cross_sections.html).

To accommodate this increase in fluorophore number, the microscope was designed to be capable of handling up to eight simultaneously acquiring photodetectors, though only four were implemented at the time of publication. Only four detectors were necessary due to a signal processing technique called Channel Subtraction and developed specifically for this

application (Kedrin *et al.*, 2007, Entenberg *et al.*, 2013). In this technique, spectrally overlapping, but somewhat shifted, fluorophores can be cleanly separated when they label spatially distinct structures. This is accomplished by choosing filters such that one of the fluorophores can be individually detected by one detector, while the second fluorophore can

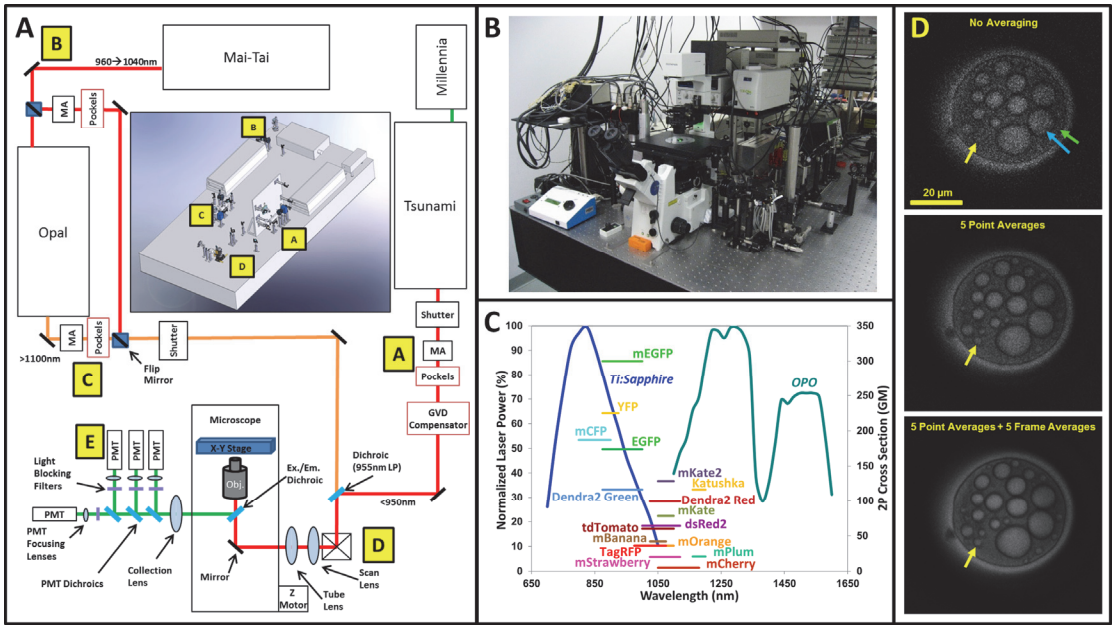

Figure 5: The two-laser multiphoton microscope. A) Optical layout of custom-built two-laser multiphoton microscope. The TLMPM provides excitation for fluorophores in the range of 750–1,040 nm and 1,100–1,600 nm and collects visible emission in four distinct channels. Light is generated by two standard femtosecond Ti:Sapphire lasers or by an optional optical parametric oscillator (OPO). The two beams then pass through scanning galvanometers into the microscope. The letters A, B, C, D, and E designate five separate functional groupings of optical components. The inset shows a computer-aided design of the entire optical layout for the two-laser multiphoton microscope showing the two laser systems and the five functional units. Note that the body of the microscope is omitted. GVD = group velocity dispersion compensator; MA = manual attenuator; Obj = objective lens; PMT = photomultiplier tube. **B)** Photograph of the two-laser multiphoton microscope. **C)** Laser output power and spectra for a Ti:Sapphire femtosecond pulsed laser and an optical parametric oscillator (OPO) along with the bandwidths and brightnesses of many commonly used fluorescent proteins. Many new fluorescent proteins cannot be efficiently excited with standard femtosecond pulsed lasers (blue curve). Use of an OPO (dark green curve) dramatically expands the useable wavelength range and increases the number of probes that may be used simultaneously. **D)** Overclocked acquisition dramatically increases signal to noise without increasing cost or sacrificing image acquisition time. A weakly fluorescent droplet of oil (green arrow) with encapsulated droplets of water (blue arrow) on a coverslip. **Top panel:** Without averaging, the low signal to noise makes some of the water droplets impossible to detect (yellow arrow). **Middle Panel:** Capturing the image with 5 point averages improves the signal to noise and reveals those structures that were hidden (yellow arrow). **Bottom panel:** Combining point averages with frame averages further increases the signal to noise and more clearly distinguishes the structures. Adapted with permission from (Entenberg *et al.*, 2011).

be detected in two channels. Gains of the two detectors are then adjusted such that the signal from the overlapping fluorophore appears equally bright in both channels. Separation is then achieved by a simple subtraction of the two channels. This results in the ability to capture, simultaneously, five to seven channels of high resolution intravital imaging data with only four detectors.

An additional feature of this microscope was a novel detection scheme that dramatically increased signal to noise of the acquired images without increasing the cost of the microscope or sacrificing acquisition time. Given that the frame rate of this microscope was ~1 fps (which for 512x512 pixel images results in a pixel clock of ~4 µs or 250 kHz), and that the time required for a single sample with the data acquisition board was ~100 ns, much of the signal emitted from the sample is lost. Capture of the complete signal throughout the pixel dwell time would require sophisticated electronic instrumentation, such as a box-car integrator, but unfortunately these instruments are typically expensive (~£8,500 per channel) and slow (~20 kHz max).

Thus, for this work I devised an alternative solution which utilises the fact that data acquisition boards can easily run at speeds nearly ten times that of the pixel clock. This “overclocking” technique allows the acquisition of five to ten data samples (acquisition clock of 10 mega-samples per second (MS/s) = 0.1 µs per sample) within the time that the laser scans over a single pixel. Averaging these samples down to a single value per pixel then results in a dramatically increased signal-to-noise ratio, is accomplished without any additional cost for hardware or increased acquisition time as all of the samples reside within a single pixel and results maintaining the acquisition frame rate of ~1 fps. The impact of this development can be seen in **Figure 5D** which shows a weakly fluorescent droplet of oil (green arrow) that contains encapsulated droplets of water (blue arrow). Without averaging (left panel), the low signal-to-noise ratio resulting from the high gain of the photomultiplier tube, makes some of the water droplets impossible to detect (left panel, yellow arrow). Point averaging (middle panel) reveals many of these structures (middle panel, yellow arrow). By combining point averaging with standard frame averaging (right panel), a dramatic improvement in signal to noise and image clarity can be achieved (lower panel, yellow arrow). The major cost of this improvement in signal to noise comes with the increased memory and processing capacity

that must be used to store and process the averaged pixels in real time. This could potentially be alleviated by performing the calculations on a field programmable gate array (FPGA).

Finally, custom written software was developed for facilitating the tracking of individual tumour cells recorded during intravital imaging. The semi-automated tracking that this software provided is crucial to the analysis of intravital imaging data since automated segmentation algorithms break down for the closely packed cells composing a tissue.

My contribution to this work included: the design and development of the microscope (including design of the mechanics, acquisition electronics, software, and laser beam path); microscope construction and use in capturing images of fluorescently labelled tumour cells in live animals; conception, design, and implementation of the overclocking scheme; and design and coding of the tracking software as a plugin for ImageJ (Schneider *et al.*, 2012).

Category 2: Novel imaging based assays to dissect the tumour microenvironment (What to look at)

Permanent FRET biosensor

Collaborating with researchers at Einstein, I worked to characterise and establish the utility of a novel photoswitchable fluorescent protein for use in multiphoton applications (Subach *et al.*, 2012). My collaborators in this work, experts in directed evolution and synthesis of fluorescent proteins, developed a novel mutated version of a monomeric protein, PSmOrange (Subach *et al.*, 2011), that they called PSmOrange2. This protein is capable of permanently switching from a state where it fluoresces with an orange colour (excitation = 546 nm, emission = 561 nm) to a state where it fluoresces with a far-red colour (excitation = 619 nm, emission = 651 nm) which happens after exposure to blue-green light (480-540 nm). In our work, we

characterised the properties of this protein, both acting alone, and as a permanent FRET biosensor.

Utilisation of this protein as a biosensor was accomplished by tagging two different interacting endogenous proteins within a cell, one with PSmOrange2, and the other with T-Sapphire (a GFP like fluorescent protein with excitation = 399 nm and emission = 520 nm) (Zapata-Hommer & Griesbeck, 2003). When the two tagged endogenous proteins interact within the cell, they come into such close contact that their fluorescent tags form a FRET pair (a donor and an acceptor protein). If the cell is illuminated with a wavelength that will excite the T-Sapphire (donor) protein (i.e. 399 nm), while the two proteins are in contact, its emission will be directly transferred to the PSmOrange2 (the acceptor) without the release of a photon. Despite the lack of photon emission, this direct energy transfer is sufficient to cause PSmOrange2 to photoswitch permanently from its orange to its far-red state.

Thus the existence in the cell of PSmOrange2 molecules capable of fluorescing in the far-red acts as a permanent (until the PSmOrange2 protein is turned over) indicator that the proteins were interacting at the time of T-Sapphire exposure. This distinguishes this FRET biosensor from any previously published FRET biosensor in two ways. Firstly, all other FRET biosensors are transient in nature, only producing a FRET signal during the time that the proteins are in contact. The consequence of this permanence is that converted proteins may be tracked over time, even if the interacting proteins subsequently separate. Secondly, all other FRET biosensors produce a FRET signal which requires careful analysis to separate the often small (~15-30%) FRET signal from the residual donor emission signal. In our implementation, all signal generated by the far-red protein is FRET signal and this fluorescence is unencumbered by background fluorescence from the donor. Quantification is accomplished simply by direct measurement of the fluorescence signal intensity of the far red form of PSmOrange2.

My contribution to this work was the characterisation of the properties of PSmOrange2 using two-photon excitation. This includes directly comparing the brightness of the new protein to its original form, PSmOrange; determining the conditions (exposure time and laser intensity) for photoswitching using a femtosecond pulsed laser; measuring the relative two-photon cross section of the protein in its orange and far-red forms; and measuring the FRET facilitated photoswitching with two-photon excitation. Additionally, I conceived of the permanence advantage of the biosensor.

Biosensor for hypoxia

Based upon this experience, I collaborated again with researchers at Einstein to develop, characterise, and utilise another biosensor for use with multiphoton microscopy. This time, the biosensor was a novel, genetically encoded fluorescent protein whose expression was driven by exposure of the cell to low levels (<1%) of oxygen (Wang *et al.*, 2016). Thus, when exposed to low oxygen levels, the cells would begin to fluoresce in a red colour.

The ability to sense when tumour cells are in the presence of low oxygen levels (hypoxia) is important in cancer research. This is because hypoxia is a common occurrence in solid tumours, arising when the uncontrolled proliferation of tumour cells makes them outgrow their vascular supply, or when the malformed neo-vasculature of a tumour is unable to sustain adequate flow to oxygenate the tissue sufficiently. Thus tumour tissues often experience oxygen levels in the range of 0.3 – 4.2% (with most tumours exhibiting median oxygen levels <2%), compared to normal tissue levels of 3 – 7.4% with a mean of ~5% (McKeown, 2014). Hypoxia in tumours results in the secretion of inflammatory and angiogenic signals that have been associated with an increased ability of cancer cells to disseminate and form metastases (Rankin & Giaccia, 2008, Brahimi-Horn *et al.*, 2007, Dunphy *et al.*, 2009). Further, many therapies currently undergoing clinical trials (e.g. Avastin) specifically target the developing tumour vasculature in an attempt to starve the cells of oxygen and nutrients (Jayson *et al.*,

2016), but they may have unwanted clinical consequences that need to be explored in more detail.

Using the biosensor developed at Einstein, we were able to measure and directly compare the motility and degradative ability of normoxic and hypoxic tumour cells both *in vitro*, and *in vivo* (Wang *et al.*, 2016). Contrary to what has been observed *in vitro* (Cuvier *et al.*, 1997), we found that, compared to normoxic cells, hypoxic tumour cells exhibit a phenotype where the they migrate with significantly reduced speeds while simultaneously being more efficient at degrading extracellular matrix and moving directionally towards blood vessels. Together, these properties make hypoxic cells possess a much more aggressive phenotype than normoxic cells leading to increased levels of tumour cell invasion and dissemination (as measured by circulating tumour cells (CTCs).

While hypoxia is generally thought of as a single state, it is actually a continuum with different biological effects becoming evident at different oxygen levels. Thus, given the rather high oxygen level for activation of the hypoxia biosensor (~1%), it is possible that the biosensor state will not correlate well with some phenotypes that only become apparent at extremely low levels of oxygen (<0.1%)

My contribution to this work included the characterisation of the biosensor using two-photon excitation; intravital imaging of the hypoxic and normoxic tumour cells in mouse mammary tumours; image analysis of the resulting time-lapse movies; and statistical analyses of the tumour cell motility.

Micro-fluidic devices for direct manipulation of tumour microenvironments

Working in collaboration with researchers at the Colleges of Nanoscale Science and Engineering in Albany, NY, I have developed and characterised an implantable microfluidic device, called the NANIVID (Nano Intravital Device) (**Figure 6A**), that is compatible with intravital multiphoton microscopy and which allows the controlled release of chemical factors into a living tumour (Williams *et al.*, 2016). This allows the direct manipulation of the tumour microenvironment with chemical factors (e.g. hypoxia, chemo-attractants, extracellular matrix alteration, chemotherapy, etc.) while imaging the results intravitally.

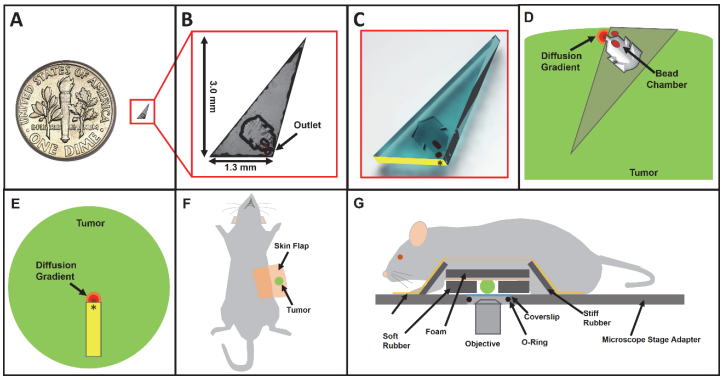

Figure 6: Nano Intravital Device (NANIVID) optimized for intravital imaging. A) Intravital imaging device next to a 17.9mm U.S. dime for reference. **B)** Micrograph of actual NANIVID with dimensions. Location of outlet at end of etched chamber is indicated. **C)** 3D computer aided design (CAD) rendering of the device. Yellow indicates back surface which is visible under the microscope. Asterisk indicates location on back surface directly adjacent to the device outlet. **D)** Schematic of a cross section of the tumour with the implanted device illustrating diffusion gradient emanating from the device outlet. Red dots indicate the fluorescent bead chambers etched into the cover. **E)** View of the tumour with implanted device as would be viewed from microscope perspective. Asterisk indicates device outlet. **F)** Supine view of a mouse after skin flap surgery to expose the underlying mammary tumour. **G)** Side view showing the tumour within the hydration chamber with the fixturing apparatus in place. Strips of hard rubber are affixed with tape to the foam backing to immobilize the tissue to the microscope stage adaptor, without causing tissue compression. NANIVID devices are inserted into the tumour and a coverslip is held in place on the microscope stage adapter with an O-ring. Adapted with permission from (Williams *et al.*, 2016).

As shown in **Figure 6B**, the microfluidic device is a 3.0 x 1.3 mm triangular sliver of glass with a hollow chamber etched into its centre that can be loaded with any chemical factor of interest. **Figure 6C** shows a three dimensional computer aided design rendering of the device with the back edge highlighted in yellow. The asterisk in this figure indicates the point on the back edge which is adjacent to the microfluidic outlet.

Use of the NANIVID for intravital imaging within solid tumours imposes strict requirements on the design of the device. Insertion into stiff tumour tissues requires a device with a small form factor (<3mm) and a sharp point. The chamber outlet is designed to be at a depth proper for

multiphoton imaging when the device is fully inserted into the tumour (back edge flush with the tissue surface), as shown in **Figure 6D**. Fluorescent beads placed in etched wells within the cover aid in locating the device outlet under the microscope. When observed from the perspective of the microscope (**Figure 6E**), the gradient can be seen to extend into the tissue where its impact on the adjacent tumour cells can be directly visualised. As a proof of concept, we used devices loaded with a chemo-attractant such as epidermal growth factor (EGF) for tumour cells (mixed with a hydrogel for controlled time-release) and imaged their response to the released gradient in real time.

We additionally used the NANIVID loaded with chemical-based hypoxia mimetics (e.g. $CoCl_2$, deferoxamine) to induce hypoxia-like responses (activation of the hypoxia inducible factor, or HIF, pathway) in solid tumours . This paved the way for application of the NANIVID, in combination with the hypoxia biosensor listed above, to look at the role hypoxia has in metastasis (Fluegen *et al.*, 2017). This work has shown that hypoxia programmes disseminated metastatic cells for dormancy and chemotherapeutic resistance.

Crucial to the ability of visualising the tissue response to the device on the single cell level, was the development of techniques for immobilising the tissue over the long periods of time required for an optimal response to develop. To address this need, I developed significant advances in stabilisation techniques for intravital imaging of tumour tissues which resulted in a 10-fold increase in acquisition time for time-lapse intravital imaging movies of mammary tumours (from 30 min to over five hours). These techniques consisted of a combination of mechanical designs and surgical protocols which gently fixture the tissues, keep them isolated from respiration, muscle, and cardiac induced vibrations imposed by the rest of the body, and maintain their hydration over extended periods of time (Entenberg *et al.*, 2017). Placing the emphasis on preventing motion artefacts during image acquisition obviates the need for nearly all post-acquisition (post-processing) software based motion artefact correction (Vinegoni *et al.*, 2014).

My contribution to this work included designing the device; developing of the tumour fixturing techniques that enabled the long-term, stable, intravital imaging; designing the instruments required to manipulate and implant the NANIVID; and performing the intravital imaging.

Automated digital pathologic analysis

As will be described in further detail in the Chapter 4, intravital imaging of sites of metastasis has identified that tumour cell intravasation occurs overwhelmingly in close association with macrophages (Wyckoff *et al.*, 2007). Thus the juxtaposition of a macrophage, a tumour cell, and an endothelial cell, a structure called the Tumour Microenvironment of Metastasis (TMEM), can be used as a marker for haematogenous dissemination in invasive breast cancer by staining for the three cell types in formalin fixed paraffin embedded tissues. TMEM density has been analysed in primary tumour samples derived from clinical cohorts using manual identification and quantification by trained pathologists (Robinson *et al.*, 2009, Rohan *et al.*, 2014) and it was shown to be prognostic for distant recurrence in invasive breast cancer, independently of classical clinicopathologic features.

Working closely with one of the pathologists, I developed and analytically validated a fully automated and scalable digital pathology/image analysis algorithm, called MetaSite Breast Score, for the identification and enumeration of TMEM sites. This automated assay demonstrated high analytical accuracy, reproducibility, and precision while reducing pathologist time by an order of magnitude, from 50 min down to 5 min (Sparano *et al.*, 2017). Analysis of MetaSite Breast Score's correlation with distant recurrence in very large patient cohorts such as E2197 (Goldstein *et al.*, 2008) showed that MetaSite is a prognostic marker for early recurrence in oestrogen receptor positive (ER+) disease and is able to provide information complementary to OncoTypeDX™ recurrence score, a standard of care prognostic test for patients with ER+ disease. MetaSite weakly correlates with OncoTypeDX™ (Pearson's Coefficient = 0.27) and is able to stratify outcome for those patients who had a low

risk OncoTypeDX™ score (<18). Comparison between the upper and lower tertile MetaSite scores for low OncoTypeDX™ scoring patients showed a 9.7-fold higher risk of distant recurrence and 6.1-fold higher risk of overall recurrence.

Thus, this study established the clinical and analytical validity of the MetaSite Breast Score as a prognostic test for metastatic outcome which provides complimentary data to the standard recurrence test, while more accurately assessing the risk in OncoTypeDX™-determined low risk patients. My contribution to this work included scanning the entire cohort on a digital whole slide scanner; developing the digital pathology algorithm, and validating its performance and reproducibility.

Category 3: Novel surgical protocols to enable ultra-high-resolution optical imaging in living animals (Where to look)

The following section describes my work developing new techniques designed to give researchers the ability to easily perform intravital imaging in extremely challenging-to-image tissues that are implicated in cancer progression and metastasis in mouse models. In particular, it details the development of surgical protocols for the exposure and stabilisation of a variety of tissues. These protocols have enabled long-term imaging of many tissues, including mammary tumours (Harney *et al.*, 2016), liver, kidney, as well as extremely compliant ones such as the untransformed mammary gland, lymphatics and lymph nodes, and the lung (Entenberg *et al.*, 2018, Harney *et al.*, 2016, Entenberg *et al.*, 2017).

Intravital imaging of mammary tumours

Working in collaboration with researchers at Einstein College of Medicine, I began my work in intravital imaging (IVI) using the two-laser multiphoton microscope described above to image solid breast cancer tumours (where the tumour cells were made to express a fluorescent protein) with the goal of studying cancer cell motility and behaviour both near and far from blood vessels (Patsialou *et al.*, 2013). Using this set up, we imaged many mammary tumours

at single cell resolution for periods of 30 minutes each. Analysis of the IVI movies identified two different tumour cell migration patterns: single cell migration, and multicellular streams of discohesive cells (i.e. tumour cells follow each other along a single path, but without cell-cell junctions between them). We further found that only the streaming cells were significantly correlated with proximity to blood vessels indicating that these cells are likely the subpopulation responsible for tumour cell intravasation and dissemination.

Intravital imaging of the untransformed mammary gland

In collaboration with researchers at Mt. Sinai Medical Centre in New York City, we looked at the molecular mechanisms that allow mammary epithelial cells to disseminate, even at stages before overt tumours exist. Using mice that express a cyan fluorescent protein (CFP) in the cells of the mammary epithelium, we performed intravital imaging in the untransformed mammary gland. Mammary gland tissue is particularly difficult to image intravitally because of its extreme compliance and proximity to the chest wall which results in the direct transmission of motion artefacts (e.g. heartbeat, breathing, twitching). To enable this imaging, I developed a fixturing technique that completely isolates the tissue from all motion and allowed long-term time-lapse, large-area mosaic, and ultra-high resolution imaging (Entenberg *et al.*, 2017). Using this technique, we were able to visualise tumour cell migration and intravasation providing direct evidence that tumour cells are able to disseminate even at the hyperplasia and ductal carcinoma *in situ* stage (Harper *et al.*, 2016).

My contribution to this work included developing the fixturing techniques; performing the intravital imaging; analysing the motility of the cells; and performing the intravital imaging.

Intravital imaging of lymphatics and lymph nodes

Using similar techniques, I collaborated with another group at Mt. Sinai Medical Centre to look at the role that chemokines expressed by lymphatic endothelial cells play in tumour cell

dissemination via the lymphovascular system (Das *et al.*, 2013). Lymphovascular invasion has traditionally been thought to be the result of tumour cells being passively carried by the lymph to the nodes, but in this study, we demonstrated that entry of tumour cells into the lymphatic sinuses of the lymph node via the afferent lymph vessels is a controlled event regulated through the expression of the chemokine CCL1 which is expressed in the sinuses, but not the peripheral lymphatics. Using techniques similar to those described above for the mammary fat pad, we imaged tumour cells in the lymphatics and in the subcapsular sinuses of the lymph nodes to examine tumour cell migration patterns. We directly observed that that tumour cells in lymphatic vessels are not carried passively by the lymph, suggesting that they arrest at the lymphatic vessel wall through an active mechanism, and not because the tumour cell emboli occluded the vessel lumen.

In this work, I developed the methods for performing the stabilised intravital imaging, analysed the motility of the cells and performed statistical analyses of the tumour cell motility.

Large-volume high-resolution intravital imaging

Imaging of the untransformed mammary gland and the lymph node required the development of several tissue stabilisation techniques to immobilise these extremely compliant tissues and eliminate all motion artefacts. An advantage of utilising these techniques was that the stabilised tissues could be imaged for much longer periods of time than the 30-minute sessions that were initially used to evaluate tumour cell motility phenotypes. The extended imaging times (up to 12 hours) proved to be essential for capturing rare events such as tumour cell intravasation (Harney *et al.*, 2015, Harper *et al.*, 2016). However, even with the additional time duration, the amount of information garnered from typical intravital imaging setup is limited to just a few randomly positioned high-resolution fields-of-view due to multiphoton microscopy’s requirement of high-numerical aperture, high-magnification objective lenses for efficient multiphoton signal generation.

Thus, while multiphoton microscopy can generate images that are reminiscent of those acquired with histopathology (**Figures 2B and 7A**, top panels), they represent only a small fraction (<1%) of the tumour's imageable area (typically ~1 cm). When placed into the context of this larger area (**Figure 7A**, bottom panel) the large amount of missing information can be readily appreciated.

To address this limitation, and dramatically increase the volume of tumour tissue recorded, I turned to a technique commonly used in digital pathology: that of large volume, high resolution (LVHR) imaging which involves the acquisition of low-magnification, high-resolution images built up by acquiring many individual, high-magnification high-resolution tiles in a sequential manner and stitching them together.

Figures 7B-D demonstrate the technique, where **Figure 7B** shows just a few high magnification fields-of-view from a well-known picture. Presented with just this limited amount of information, it is exceedingly difficult to discern the subject underlying the images. Acquiring more fields-of-view, even to the point of complete coverage, improves the information garnered (for example, the subject is a person, the subject is a Caucasian person, the person has white hair, etc.), however some characteristics are still difficult to discern (e.g. Is the subject a male or female?) and identification of the subject is still challenging (**Figure 7C**).

Only by acquiring all of the fields-of-view in a particular order and maintaining their spatial relationships (**Figure 7D**, black arrows indicate order of acquisition) can the complete image be reconstructed and the identity of the subject revealed.

This technique is very commonly utilised in diverse fields such as biology (De Zanet *et al.*, 2016, Seshamani *et al.*, 2006), oceanography (Kwasnitschka *et al.*, 2016), and X-ray microscopy (Loo *et al.*, 2000), but had been more rarely used with multiphoton microscopy, and then, only with fixed tissues (Price *et al.*, 2006). Indeed, the acquisition of LVHR images is simple and straightforward when motion of the sample is not present. The limitation to successful combination of LVHR imaging with intravital imaging lies not in the hardware or instrumentation, but in the ability to stabilise the living tissues sufficiently in the presence of the many motion artefacts that arise in a living animal such as breathing, heartbeat, muscle twitching, and tissue dehydration.

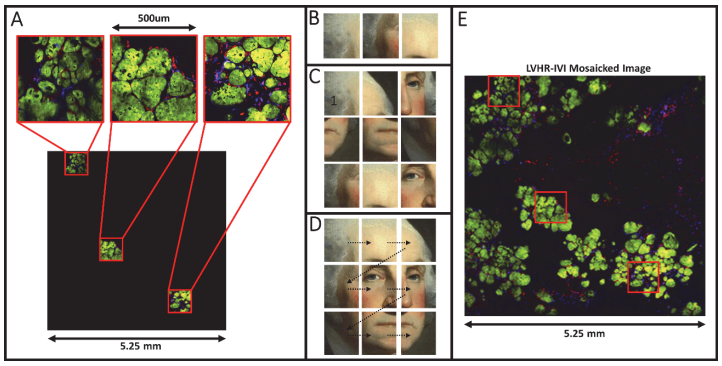

Figure 7: Large-volume high-resolution intravital imaging (LVHR-IVI). A) The optical sectioning capabilities of multiphoton microscopy produce high-resolution, high-magnification images (top panels), however back-projecting these field of view onto the entire tissue (bottom panel) shows that they span a small percentage of the whole tumour. Green = GFP labelled tumour cells, red = 155kD labelled vasculature. **B)** Small sections from a well-known image do not provide enough context to fully understand the imaged subject. **C)** Additional images improve the information garnered, but still do not reveal the identity of the subject. **D)** Acquiring the high-resolution images in a particular order (black arrows) and maintaining their spatial relationships allows stitching together of the full image and identification of the subject. **E)** LVHR-IVI captures the information missing from **A)** and reveals the tissue to be early stage carcinoma. Green = GFP labelled tumour cells, red = 155kD labelled vasculature. Red boxes indicate the fields-of-view from **A)**. Adapted with permission from (Entenberg *et al.*, 2017).

Stability of the sample is particularly important for LVHR with images from microscopes, as movements on the order of microns can distort and blur a high resolution image. Only through the use of the stabilisation techniques described above, is it possible to combine LVHR imaging with intravital imaging, a technique we have called Large Volume High Resolution Intravital Imaging (LVHR-IVI). The successful application of this technique to a living mouse

is shown in **Figure 7E** which reveals the rest of the tissue missing in **Figure 7A** and enables the determination of the stage and grade of this tumour. The red boxes indicate the individual fields-of-view displayed in **Figure 7A**.

Thus, these time-lapsed multiscale images can allow a much more complete investigation of cellular dynamics than is possible with ordinary intravital imaging. Further, the images generated with LVHR-IVI become usable in the same manner that pathologists utilise microscopy to diagnose disease states in tissues and organs where high-magnification images are used to identify the staining and morphology of individual cells and low-magnification overviews are used to determine their context and location. However, LVHR-IVI goes beyond these capabilities by adding in the dynamics of the living tissue revealing real-time events such as cell-cell and cell-stroma interactions.

To my knowledge our publication on dissemination of cancer cells at very early stages (before overt tumours are detectable), which relied heavily on LVHR-IVI for imaging the untransformed mammary gland, represented the first report in the literature to utilise LVHR-IVI with live tissues (Harper *et al.*, 2016).

For this work, I designed and developed the surgical protocols for stabilisation of a variety of tissues, conceived of the technique of large-volume high-resolution intravital imaging, and performed the intravital imaging and image analysis (Harper *et al.*, 2016, Entenberg *et al.*, 2017).

Intravital imaging of the lung – Vacuum stabilised imaging window

One of the most common sites of metastatic dissemination are the lungs (Lee, 1983). However, the lungs are delicate, vital organs positioned deep within the body and in constant motion, making them arguably the most difficult organs to visualise using intravital imaging. As a result, the vast majority of studies of lung metastases have utilised either fixed or *ex vivo*

preparations which only give a view into the lung at single time points (Qian *et al.*, 2009, Al-Mehdi *et al.*, 2000, Cameron *et al.*, 2000). These studies do not give a complete understanding of the interactions and dynamics that occur between the various components of the lung parenchyma. Further, separating the lungs from the circulatory system leads to a dramatic imbalance of homeostasis and disconnects the tissue from the body's immune system, preventing the influx of immune cells that may be part of the physiological response crucial to tumour cell survival, extravasation, and growth.

To address these limitations, I, along with collaborators at Einstein College of Medicine, developed a vacuum stabilised imaging window (Entenberg *et al.*, 2015) and surgical protocol (Rodriguez-Tirado *et al.*, 2016) for utilising it to perform long-term (up to 12 hours) intravital imaging of the lungs. The surgical protocol, shown schematically in **Figure 8A**, involves intubation and mechanical ventilation of the mouse with a tracheal catheter followed by resection of a portion of the thoracic cavity wall to expose the lung tissue. The exposed lung tissue is then placed against a custom designed vacuum window which is connected to a vacuum hose as shown in **Figure 8B**. In this design, the vacuum window stabilises the lung tissue relative to the window, but motion from contraction of the intercostal muscles may still be transmitted to the entire window and cause a positional shift relative to the microscope's objective lens. Thus, our design also included a fixturing plate that attaches to the microscope's xy stage plate and completely immobilises the window relative to the objective lens (**Figure 8C**).

The complete immobilisation of the tissue, combined with optimisations to performance of the microscope (e.g. optimised signal-to-noise through improved multiphoton signal generation and amplification electronics), enabled ultra-high resolution optical imaging of metastasised tumour cells, leading to the visualisation of membrane dynamics, chromosomal separation, and interactions with resident macrophages. **Figure 8D** shows frames from a time-lapse move in which a single cell can be observed to divide in the lung. Condensed chromosomes, which

are readily visible by their exclusion of the cytoplasmic GFP, can be seen to undergo alignment (yellow arrow at t=0') and separation (yellow arrows at t=4' and t=8'), after which the cell separates (blue arrow at t=10') into two daughter cells.

For this work, I designed and developed the imaging window and fixturing plate; developed the surgical protocol; performed the surgery, performed the intravital imaging; and designed and implemented the microscope optimisations that allowed the capture of subcellular events.

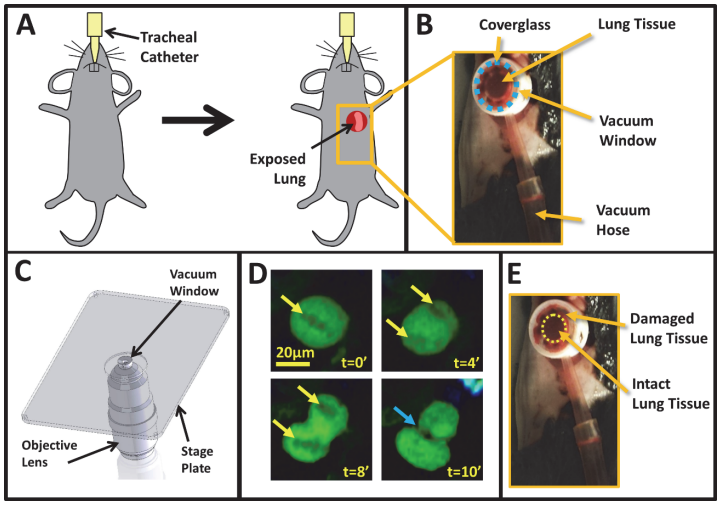

Figure 8: Vacuum stabilized and implantable lung imaging windows. A) Surgical protocol for exposing the lung involves intubating and mechanically ventilating the mouse using a tracheal catheter followed by resection of the chest wall to expose the lung tissue. **B)** Picture of the vacuum window attached to the lung. Vacuum applied to the window via a vacuum hose adheres the lung tissue to the cover glass (indicated by the dotted blue line) and immobilizes the tissue relative to the window. **C)** 3D computer aided design drawing of the vacuum window placed into the imaging stage plate and positioned relative to the microscope's objective lens. **D)** The high spatial stability of the tissue allows single cell imaging with sufficient resolution to enable visualization of subcellular structures such as chromosomal alignment (yellow arrow in t=0' frame) and separation (yellow arrows in t=4 and t=8' frames) followed by membrane pinching (blue arrow in t=10' frame) and separation of the two daughter cells. Green = E0771-GFP tumour cells, Blue = CFP labelled macrophages. **E)** The vacuum stabilized imaging window keeps the immobilized lung tissue intact within the imaging zone (inside of yellow dashed circle), however tissue bordering this region is damaged by the vacuum channels in the window. Adapted with permission from (Entenberg *et al.*, 2015).

Intravital imaging of the lung – Permanent window for high resolution imaging of the lung (WHRIL)

While the vacuum stabilised imaging window described above provided the first ever high-resolution view of tumour cells in the lung vasculature, the technique is limited in several ways. First, since the surgical protocol breaches the seal of the thoracic cavity, the lung tissue is exposed to non-physiological levels of gasses which can alter the biological processes under investigation. Second, the use of vacuum for stabilisation of the lung tissue is potentially problematic as this may lead to artefacts of compression or restricted vascular flow.

Third, the surgical protocol is extremely invasive, involving resection of about a third of the chest wall and physically contacting the lung with the vacuum imaging window. While this keeps the lung viable and intact within the imaging region (**Figure 8E** inside the yellow dashed circle), the surrounding lung tissue is significantly damaged by contact with the vacuum ports within the window (**Figure 8E** outside of the yellow dashed circle). Thus it is impossible to have the mouse survive beyond a single imaging session (which is itself limited in duration to <12 hrs). Given that the metastatic cascade takes days to weeks to occur, the vacuum window allows only brief glimpses into dynamics of cancer cell dissemination.

This last limitation is particularly significant since it precludes the study of tumour cells which have spontaneously metastasised from a primary tumour. Without the ability to view the tissue over multiple days, it is impossible to tell when the cells have arrived to the lung vasculature, and hence, what their natural history is. To avoid this, traditional studies of metastasis,

including imaging studies, have relied upon the introduction of tumour cells to the lungs by the direct infusion into the circulatory system of cells taken straight from cell culture, a technique called "experimental metastasis" that has been utilised for over a hundred years (Levin & Sittenfield, 1911).

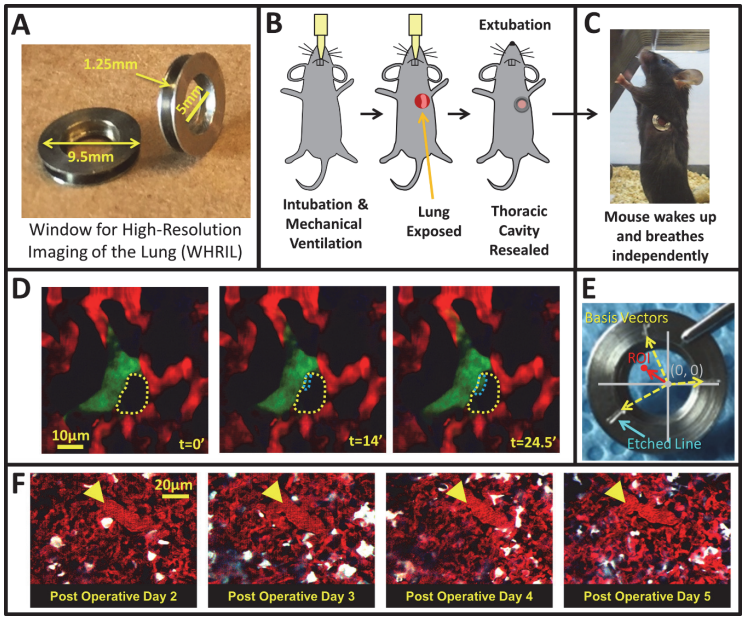

Figure 9: Window for High-Resolution Imaging of the Lung (WHRIL). **A)** The WHRIL is a 9.5 mm stainless steel disc with a 1.25 mm radial groove and a recessed aperture that accepts a 5 mm cover glass. When implanted into the chest wall of a mouse, the rib cage fits snugly into the groove and the cover glass seals the aperture forming an air tight closure. **B)** Schematic of the surgical protocol. After intubation and mechanical ventilation, the chest wall is breached and the lung tissue exposed by cutting a small (~5 mm) circular hole. The WHRIL frame is then implanted and the thoracic cavity resealed with a combination of suture and adhesives. **C)** Resealing of the thoracic cavity means that the mouse can be extubated, recover from anaesthesia, and breathe independently. Validation experiments showed that the window is well tolerated allowing the mouse to resume normal daily activities with ease. **D)** High resolution, single-cell optical imaging of the living breathing lung tissue can be accomplished through the window. The technique allows direct visualization of the dynamics of disseminated tumour cells over time in the lung. Three stills taken from a time-lapse movie of a single cell 24 hours after arrival in the lung vasculature show the cell beginning to cross the endothelial wall into an adjacent alveolus (yellow dotted lines). The blue dotted lines at t=14' and t=24.5' indicate the extravascular portion of the tumour cell. Green = E0771-GFP tumour cells, Red = 155kD fluorescent Dextran labelled blood vessels. **E)** Microcartography can be used to find the same microvasculature on serial imaging sessions. Fiducial marks are etched into WHRIL frame (cyan arrow). These locations form a set of basis vectors (yellow arrows) which can be used to calculate a coordinate transform relating the locations of any arbitrary region of interest (ROI, red dot and red arrow) on subsequent days. **F)** Microcartography successfully relocates the same vasculature (yellow arrow heads) day after day. Adapted with permission from (Entenberg *et al.*, 2018).

To address these limitations, I developed a mechanical design and minimally invasive surgical protocol for implanting an optical imaging window permanently into the chest wall of a mouse.

The window, which we call the Window for High-Resolution Imaging of the Lung (WHRIL), is shown in **Figure 9A** and consists of a 9.5 mm diameter stainless steel frame which accepts a 5 mm cover glass into its central aperture. A 1.25 mm groove around the border is recessed so as to capture and create a seal around the ribcage of the mouse when implanted into the chest wall.

The surgical protocol for implantation, outlined in schematic form in **Figure 9B**, begins, just like the vacuum window protocol, with intubation and mechanical ventilation of the mouse. However, in this case, a combination of sutures and adhesives enables the implanted window to completely reseal the thoracic cavity, allowing the mouse to breathe independently and recover from anaesthesia.

A series of validation experiments demonstrated that the window is well tolerated, produces no local or systemic inflammation and that the mice are able to continue their normal routine and live comfortably with the implanted window for weeks (Entenberg *et al.*, 2018). **Figure 9C** shows that the mouse is healthy and able to stretch and reach for food with ease.

Just as with the vacuum window, the WHRIL enables high-resolution single-cell intravital imaging of the lung. **Figure 9D** shows stills from a time-lapse movie of a single tumour cell two days after injection into the vasculature. The cell, which is still intravascular, extends protrusions through the endothelial wall into the adjacent alveolar space (outlined with a yellow dashed line). For clarity, the protrusion has been outlined with a blue dashed line in the t=14' and t=24.5' panels.

Unlike the vacuum window however, the permanence of the WHRIL means that imaging of the lung tissue can be performed not just in a single imaging session, but with multiple imaging sessions spanning weeks, with the mouse able to recover from anaesthesia between these sessions. However, having the mouse awaken between imaging sessions presents another challenge. As the lung tissue is a dense, fairly uniform meshwork of capillaries, arbitrary translations and rotations of the window that occur each time the mouse is removed from the microscope stage and replaced make identifying and re-localising the same micro-vessel by eye in each imaging session impossible.

To address this challenge and make the re-localisation of any arbitrary region of interest (ROI) semi-automated, I adopted the technique of microcartography which I had previously published in the context of imaging vascular degeneration after radiotherapy (Dunphy *et al.*, 2009). Microcartography relies upon the localisation of three, easily identifiable, non-collinear points which remain fixed relative to the ROIs. With the WHRIL, this is accomplished by the addition of three lines etched 120 degrees apart into the frame (**Figure 9E**, cyan arrow). The xy coordinates of these fiducial marks relative to the xy stage's origin and axes (**Figure 9E**, grey dot and lines, respectively) in each imaging session then form a set of basis vectors (**Figure 9E**, yellow arrows) which can be used to calculate a coordinate transformation and predict the location of an ROI (**Figure 9E**, red dot and arrow) in each imaging session based upon its coordinates in the previous session. **Figure 8F** shows the successful application of microcartography and the re-localisation of the same micro-vessel on four imaging sessions spanning as many days.

For this work, I designed and developed the WHRIL and its surgical protocol, adopted the microcartography algorithm, automated its use by writing a software calculator, and designed the validation experiments.

Having the ability to perform high-resolution optical imaging in metastatic sites such as the lungs (the most common site of metastasis in breast cancer) over days to weeks, will enable identification of commonalities between metastases and the primary tumours from which they derive, discovery of the mechanisms by which pre-metastatic niche formation affects tumour cell fate in the lung, and observation of differences between experimental and spontaneous lung metastatic seeding and progression.

Other intravital imaging

I have developed and written numerous protocols and book chapters on intravital imaging of mammary tumours in mice (Harney *et al.*, 2016, Entenberg *et al.*, 2013, Hulit *et al.*, 2012,

Wyckoff *et al.*, 2011, Gligorijevic *et al.*, 2010) and these techniques have enabled in many other studies of primary tumours which have discovered the role of the tumour microenvironment in dissemination and metastasis (Szulczewski *et al.*, 2016, Patsialou *et al.*, 2015, Harney *et al.*, 2015, Patsialou *et al.*, 2013).

Chapter 4: Biological discoveries about metastatic progression

The results described in Chapter 3 have enabled a number of biological discoveries into the process of metastatic dissemination of tumour cells, particularly in breast cancer. This work has investigated the interaction between tumour and stromal cells and the impact that the tumour microenvironment has on their lymphatic and haematogenous dissemination. This chapter will give a brief outline of the process of metastasis and then summarise the unique findings that were made utilising the photonics based approaches I described earlier.

The process of metastasis has been studied for over 100 years (Langenbeck, 1841), and the basic steps of the disease progression have been enumerated (Talmadge & Fidler, 2010). Crucial to this process is cancer cell motility, invasion of the vascular basement membrane, and intravasation. Using intravital imaging of GFP expressing breast cancer cells orthotopically injected into rats, Farina et al. was able to visualise the motility of cells within the primary tumour directly (Farina *et al.*, 1998). They observed that, surprisingly, the vast majority of tumour cells were stationary with only a small fraction of the cancer cells observed to be motile.

These motile cells were further observed to move together, without cell-cell junctions, at high velocity (>3 μm/min) compared to in vitro cultures (~0.1 μm/min (Lehmann *et al.*, 2017)) and in single-file streams along collagen fibres, (Farina *et al.*, 1998). This mode of migration, called streaming migration, has been observed not only in xenografts of immortalised tumour cell lines, but also in genetically engineered mouse models of breast cancer (Wang *et al.*, 2004) which have the advantage of recapitulating the tissue structure and morphology observed in the clinical disease (Lin *et al.*, 2003).

Further imaging showed that in tumours formed from cell lines that metastasise, carcinoma cells showed a greater orientation towards blood vessels (Wang *et al.*, 2002) and a

significantly lower rate of fragmentation upon intravasation compared to non-metastatic tumour cell lines (Wyckoff *et al.*, 2000a).

Utilising “artificial blood vessels” (microneedles filled with chemoattractant growth factors inserted into the tumour), *in vivo* isolation and collection of the motile, chemotaxis-competent fraction of the tumour was made possible (Wyckoff *et al.*, 2000b). These experiments revealed that macrophages and cancer cells chemotax together utilising a paracrine loop involving macrophage-derived epidermal growth factor (EGF) and carcinoma cell-derived colony-stimulating factor-1 (CSF-1) and that blocking of either factor has the effect eliminating chemotaxis of both cell types (Wyckoff *et al.*, 2004).

Collected cells were then expression profiled in order to determine which proteins within this migrating subpopulation were differentially expressed compared to the rest of the bulk tumour. Among the set of proteins that were upregulated, the Ena/Vasp family protein Mena, an actin regulatory protein highly conserved across species (Krause *et al.*, 2003), stood out as being significantly upregulated (Wang *et al.*, 2004).

Investigations into the role that the Mena gene plays showed that deleting Mena from tumour cells in animal models of cancer suppressed intravasation, eliminated mortality and morbidity, and greatly reduced the frequency of metastatic dissemination to the lung (Roussos *et al.*, 2010).

The Mena protein additionally matures into several splice-variant isoforms (Goswami *et al.*, 2009, Shapiro *et al.*, 2011) which includes Mena11a, an isoform which causes the formation of poorly metastatic tumours with a more normal epithelial architecture (e.g. tight cell-cell junctions) when expressed in breast cancer cells, and MenaINV, an isoform high associated with a more migratory, invasive phenotype (Roussos *et al.*, 2011). Tumours with cells upregulated for Mena11a are not capable of responding to EGF chemotactic cues in vivo

(Roussos *et al.*, 2011). The relative ratios of the different Mena isoforms thus can be used as an indicator of the metastatic potential of a particular tumour. This concept was captured in a multiplexed quantitative immunofluorescence test called MenaCalc which reflects the presence of metastatic competent tumour cells and has been shown to correlate with increased metastatic risk in patient cohorts (Agarwal *et al.*, 2012, Forse *et al.*, 2015).

Based upon the above mentioned observations, macrophages and tumour cells were simultaneously labelled with fluorescence for direct visualisation of their interaction in tumours *in vivo*. In this model, motile tumour cell streams were observed to contain co-opted macrophages which migrated together with the tumour cells toward blood vessels (Wang *et al.*, 2002).

At the blood vessels, intravital imaging of the transendothelial crossing event process showed that successful tumour cell intravasation overwhelmingly occurs in close proximity to macrophages (Wyckoff *et al.*, 2007).

From this work, it came to be recognised that the confluence of a Mena over-expressing tumour cell, a macrophage, and an endothelial cell, all in juxtaposition, could be utilised as a marker for locations that act as portals for tumour cell entry into the vasculature and thus for haematogenous dissemination. This confluence of cell types thus came to be termed the Tumour Microenvironment of Metastasis (TMEM) (Robinson *et al.*, 2009) and the density of TMEM (count per area of tumour tissue) in patient samples has since been shown to be prognostic for metastatic outcome in several clinical cohorts (Robinson *et al.*, 2009, Rohan *et al.*, 2014, Sparano *et al.*, 2017).

After the creation of the two-laser multiphoton microscope and the tissue stabilisation techniques detailed in Chapter 3, it was possible to perform long-term high-resolution multiphoton intravital imaging of TMEM sites. This imaging revealed that these tripartite

structures are found predominantly at vascular branch points and that they are relatively stationary constructs that persist for extended periods of time (>5hrs) (Harney *et al.*, 2015). The cell-cell contact that occurs in TMEM results in the formation of tumour cell invadopodia, extracellular matrix degrading structures (Roh-Johnson *et al.*, 2014, Gligorijevic *et al.*, 2014). These invadopodia work in conjunction with VEGF released by the macrophage to open a gap in the vascular wall resulting in transient leakage of blood serum into the interstitium. Intravital imaging was able to visualise a high rate of tumour cell intravasation concurrent with, and spatially adjacent to, this transient vascular leakage.

To prove that TMEM are truly responsible for this vascular leakage and intravasation, experiments were performed to either ablate macrophages or delete the VEGF gene. In either case, transient vasculature leakage and intravasation of tumour cells were dramatically reduced (Harney *et al.*, 2015). As further evidence, TMEM function was blocked using rebastanib, a small molecule inhibitor of Tie2 kinase activity, in orthotopic mouse models of metastatic mammary carcinoma. Treatment correlated with reduced tumour growth and distant metastasis through the reduction of Tie2+ myeloid cell infiltration, anti-angiogenic effects, and blockade of tumour cell intravasation mediated by perivascular $Tie2^{Hi}$/$VEGFA^{Hi}$ macrophages in TMEM. When used in combination with microtubule inhibiting chemotherapeutic agents, rebastinib enhanced their efficacy reducing tumour volume and distant metastasis and improving overall survival (Harney *et al.*, 2017).

Finally, after development of the implantable lung imaging window, I was able to visualise the same transient vascular leakage adjacent to TMEM within lung metastases (Entenberg *et al.*, 2018). This suggests that TMEM can be responsible for re-dissemination of tumour cells from the secondary site back into the circulation resulting in haematogenous spread to other locations within the secondary site, or on to tertiary locations. This has significant implications for the potential benefit of rebastinib in metastatic patients even after the primary tumour has been resected. Indeed, work is currently underway in the form of a Phase 1B clinical trial to

evaluate the combination of rebastinib with standard chemotherapies (Clinical trials study number NCT02824575: “Rebastinib Plus Antitubulin Therapy with Paclitaxel or Eribulin in Metastatic Breast Cancer”).

Taken together, these discoveries create a new model for how tumour cells metastasise and disseminate haematogenously. This model is summarised in **Figure 10** wherein a small number of cancer cells within the bulk tumour become migratory via a change in balance of Mena protein isoforms. These cells then pair with macrophages via a paracrine loop and travel at high speeds along collagen I fibres towards blood vessels. Once at a blood vessel, the two cells either interact with, or form a new TMEM structure which allows other streaming cells to intravasate and spread to distant sites through the blood vasculature (**Figure 10A**). Arrival to a secondary site traps the tumour cells by physical lodgement in the capillaries. Tissue resident macrophages in the secondary site then aid the tumour cells in crossing the endothelium and entering the parenchyma where resumption of growth may follow. With time, extravasated cells will develop into macro-metastases supported by either neo-angiogenic vessels, or co-opted secondary site vasculature. These vessels may then serve as sites for the formation of new, secondary site TMEM structures that recapitulate the process of the primary tumour and lead to re-dissemination of cancer

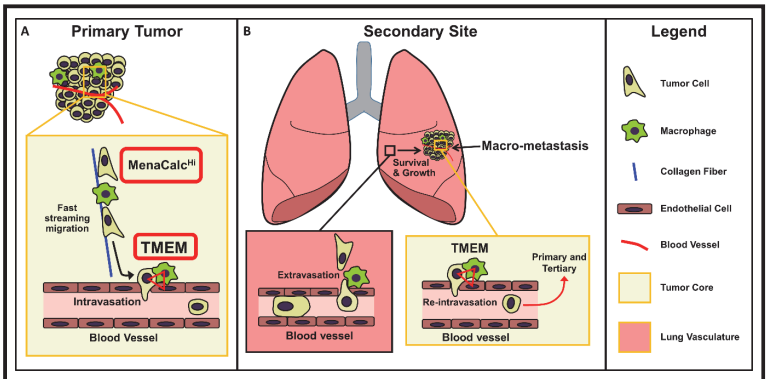

Figure 10: Technological developments lead to a new model of metastasis. A) In the primary tumour a small fraction of the tumour cells express a combination of Mena protein isoforms characterized as MenaCalc^{Hi} and begin migrating. Within the tumour core these tumour cells pair with macrophages and travel together along collagen fibres towards blood vessels. Once reaching a blood vessel, these cell pairs can form a new TMEM structure, or interact with a pre-existing one (red triangle). These TMEM structures then serve as the doorway into the vasculature where other migrating tumour cells may then intravasate and disseminate to secondary sites such as the lung. **B)** In the secondary site, the disseminated tumour cells become stuck in small capillaries due to physical size restriction until they extravasate, potentially aided by macrophages. Once in the parenchyma tumour cells may survive for some time before reinitiating growth. After growing into a macro-metastasis, blood vessels in the macro-metastasis core can then support secondary-site TMEM allowing re-intravasation and dissemination back to the primary site, or onward to tertiary sites.

cells back to the primary location, to new locations in the secondary site, or on to tertiary sites (**Figure 10B**).

Chapter 5: Conclusion

Throughout history, physics and engineering have brought about technological advances that have transformed biological research, enabling the execution of definitive tests of biological concepts and hypotheses. The work presented in this thesis applies physics and engineering principles to develop photonics based assays for biological research, with a particular focus on the field of cancer metastasis.

Understanding the process of metastasis is crucial to improving patient care. This is reflected in the current 10-year survival rates for the most common type of cancer, breast cancer. If early diagnosis detects the disease when the cancer cells are still localised in the ducts of the breast, known as localised disease, the 10-year survival rate is high, ~93%. Survival rates drop modestly, but remains fairly high at 73%, for regional disease where the tumour cells have moved beyond the boundary of their containing basement membrane. However, in the case of metastatic disease where the cancer has spread to distant sites such as the liver, the brain, or the lung, 10-year survival rates precipitously drop down to 17% (Narod *et al.*, 2015).

To address this need, I have developed assays that fall into three major categories including: 1) novel microscope instrumentation; 2) novel imaging based assays to dissect the tumour microenvironment; and 3) novel surgical protocols to enable ultra-high-resolution optical imaging in living animals. Taken together, the publications composing this work have enabled studies into tumour cell motility phenotypes and intravasation mechanisms that have led to new diagnostics and therapeutics currently being developed for use in the clinic.

My latest work, that of Large-Volume High-Resolution Intravital Imaging combined with the Window for High Resolution Imaging of the murine Lung promises to provide answers to many questions and controversies surrounding the arrival, survival, and growth of tumour cells in the lung by directly observing the process *in vivo* and in real time. These include: What factors influence the efficiency of disseminated tumour cell survival? (Fidler, 1970, Cameron *et al.*,

2000); Do circulating tumour cell clusters really develop more readily into metastases compared to single cells? (Liotta *et al.*, 1974, Cheung & Ewald, 2016); Do tumour cells need to extravasate or are they able to grow intravascularly into metastases? (Qian *et al.*, 2009, Al-Mehdi *et al.*, 2000); How do tumour cells home to different tissues? (Proctor, 1976, Hart, 1982); Does surgical resection of a primary tumour significantly contribute to the development of metastases? (Katharina, 2011, Camara *et al.*, 2006); and Do metastases co-opt the lung vasculature in lieu of inducing angiogenesis and is this a route of failure for anti-angiogenic therapies? (Bridgeman *et al.*, 2017, Ebos & Kerbel, 2011)

It is anticipated that answering questions such as these, in a definitive and direct manner, will have an immediate and significant impact upon how the therapies and diagnostics for metastatic disease are developed and applied in the clinic.

Bibliography

Agarwal, S., F.B. Gertler, M. Balsamo, J.S. Condeelis, R.L. Camp, X. Xue, J. Lin, T.E. Rohan & D.L. Rimm, (2012) Quantitative assessment of invasive mena isoforms (Menacalc) as an independent prognostic marker in breast cancer. *Breast cancer research : BCR* **14**: R124.

Aguirre-Ghiso, J.A., (2007) Models, mechanisms and clinical evidence for cancer dormancy. *Nature reviews. Cancer* **7**: 834-846.

Al-Mehdi, A.B., K. Tozawa, A.B. Fisher, L. Shientag, A. Lee & R.J. Muschel, (2000) Intravascular origin of metastasis from the proliferation of endothelium-attached tumor cells: a new model for metastasis. *Nat Med* **6**: 100-102.

Ambrose, E.J., (1956) A surface contact microscope for the study of cell movements. *Nature* **178**: 1194.

Andresen, V., S. Alexander, W.M. Heupel, M. Hirschberg, R.M. Hoffman & P. Friedl, (2009) Infrared multiphoton microscopy: subcellular-resolved deep tissue imaging. *Curr Opin Biotechnol* **20**: 54-62.

Bergers, G. & D. Hanahan, (2008) Modes of resistance to anti-angiogenic therapy. *Nature reviews. Cancer* **8**: 592-603.

Bosma, G.C., R.P. Custer & M.J. Bosma, (1983) A severe combined immunodeficiency mutation in the mouse. *Nature* **301**: 527-530.

Botstein, D., (2010) Technological innovation leads to fundamental understanding in cell biology. *Mol Biol Cell* **21**: 3791-3792.

Boyd, R., (2008) Nonlinear Optics 3rd edn (New York: Academic).

Brahimi-Horn, M.C., J. Chiche & J. Pouyssegur, (2007) Hypoxia signalling controls metabolic demand. *Curr Opin Cell Biol* **19**: 223-229.

Bravo-Cordero, J.J., L. Hodgson & J. Condeelis, (2012) Directed cell invasion and migration during metastasis. *Curr Opin Cell Biol* **24**: 277-283.

Bridgeman, V.L., P.B. Vermeulen, S. Foo, A. Bilecz, F. Daley, E. Kostaras, M.R. Nathan, E. Wan, S. Frentzas, T. Schweiger, B. Hegedus, K. Hoetzenecker, F. Renyi-Vamos,

E.A. Kuczynski, N.S. Vasudev, J. Larkin, M. Gore, H.F. Dvorak, S. Paku, R.S. Kerbel, B. Dome & A.R. Reynolds, (2017) Vessel co-option is common in human lung metastases and mediates resistance to anti-angiogenic therapy in preclinical lung metastasis models. *J Pathol* **241**: 362-374.

Camara, O., A. Kavallaris, H. Noschel, M. Rengsberger, C. Jorke & K. Pachmann, (2006) Seeding of epithelial cells into circulation during surgery for breast cancer: the fate of malignant and benign mobilized cells. *World J Surg Oncol* **4**: 67.

Cameron, M.D., E.E. Schmidt, N. Kerkvliet, K.V. Nadkarni, V.L. Morris, A.C. Groom, A.F. Chambers & I.C. MacDonald, (2000) Temporal progression of metastasis in lung: cell survival, dormancy, and location dependence of metastatic inefficiency. *Cancer Res* **60**: 2541-2546.

Castle, W.E. & C.C. Little, (1909) The Peculiar Inheritance of Pink Eyes among Colored Mice. *Science* **30**: 313-314.

Cheung, K.J. & A.J. Ewald, (2016) A collective route to metastasis: Seeding by tumor cell clusters. *Science* **352**: 167-169.

Curtis, C., (2015) Genomic profiling of breast cancers. *Curr Opin Obstet Gynecol* **27**: 34-39.

Cuvier, C., A. Jang & R.P. Hill, (1997) Exposure to hypoxia, glucose starvation and acidosis: effect on invasive capacity of murine tumor cells and correlation with cathepsin (L + B) secretion. *Clin Exp Metastasis* **15**: 19-25.

Das, S., E. Sarrou, S. Podgrabinska, M. Cassella, S.K. Mungamuri, N. Feirt, R. Gordon, C.S. Nagi, Y. Wang, D. Entenberg, J. Condeelis & M. Skobe, (2013) Tumor cell entry into the lymph node is controlled by CCL1 chemokine expressed by lymph node lymphatic sinuses. *The Journal of experimental medicine* **210**: 1509-1528.

De Zanet, S., T. Rudolph, R. Richa, C. Tappeiner & R. Sznitman, (2016) Retinal slit lamp video mosaicking. *Int J Comput Assist Radiol Surg* **11**: 1035-1041.

DeClerck, Y.A., K.J. Pienta, E.C. Woodhouse, D.S. Singer & S. Mohla, (2017) The Tumor Microenvironment at a Turning Point Knowledge Gained Over the Last Decade, and

Challenges and Opportunities Ahead: A White Paper from the NCI TME Network. *Cancer Res* **77**: 1051-1059.

Denk, W., J.H. Strickler & W.W. Webb, (1990) Two-photon laser scanning fluorescence microscopy. *Science* **248**: 73-76.

Dovas, A., B. Gligorijevic, X. Chen, D. Entenberg, J. Condeelis & D. Cox, (2011) Visualization of actin polymerization in invasive structures of macrophages and carcinoma cells using photoconvertible beta-actin-Dendra2 fusion proteins. *PLoS One* **6**: e16485.

Drobizhev, M., N.S. Makarov, T. Hughes & A. Rebane, (2007) Resonance enhancement of two-photon absorption in fluorescent proteins. *J Phys Chem B* **111**: 14051-14054.

Drobizhev, M., N.S. Makarov, S.E. Tillo, T.E. Hughes & A. Rebane, (2011) Two-photon absorption properties of fluorescent proteins. *Nat Methods* **8**: 393-399.

Drobizhev, M., S. Tillo, N.S. Makarov, T.E. Hughes & A. Rebane, (2009) Absolute two-photon absorption spectra and two-photon brightness of orange and red fluorescent proteins. *J Phys Chem B* **113**: 855-859.

Dunphy, M.P., D. Entenberg, R. Toledo-Crow & S.M. Larson, (2009) In vivo microcartography and subcellular imaging of tumor angiogenesis: a novel platform for translational angiogenesis research. *Microvasc Res* **78**: 51-56.

Ebos, J.M. & R.S. Kerbel, (2011) Antiangiogenic therapy: impact on invasion, disease progression, and metastasis. *Nature reviews. Clinical oncology* **8**: 210-221.

Enderle, J.D. & J.D. Bronzino, (2012) *Introduction to biomedical engineering,* p. xv, 1252 p. Elsevier/Academic Press, Amsterdam ; Boiston.

Entenberg D, Roorda RD & Toledo-Crow R, (2004) Non-linear microscope for imaging of the neural systems in live drosophila. In: OSA BioMed pp.

Entenberg, D., I. Aranda, Y. Li, R. Toledo-Crow, D. Schaer & Y. Li, (2006) Multimodal microscopy of immune cells and melanoma for longitudinal studies. *Proc of SPIE* **6081**: 62-73.

Entenberg, D., D. Kedrin, J. Wyckoff, E. Sahai, J. Condeelis & J.E. Segall, (2013) Imaging tumor cell movement in vivo. In: Curr Protoc Cell Biol. pp. Unit19 17.

Entenberg, D., J.M. Pastoriza, M.H. Oktay, S. Voiculescu, Y. Wang, M.S. Sosa, J. Aguirre-Ghiso & J. Condeelis, (2017) Time-lapsed, large-volume, high-resolution intravital imaging for tissue-wide analysis of single cell dynamics. *Methods* **128**: 65-77.

Entenberg, D., C. Rodriguez-Tirado, Y. Kato, T. Kitamura, J.W. Pollard & J. Condeelis, (2015) In vivo subcellular resolution optical imaging in the lung reveals early metastatic proliferation and motility. *Intravital **4***: 1-11.

Entenberg, D., S. Voiculescu, P. Guo, L. Borriello, Y. Wang, G.S. Karagiannis, J. Jones, F. Baccay, M. Oktay & J. Condeelis, (2018) A permanent window for the murine lung enables high-resolution imaging of cancer metastasis. *Nature Methods* **15**: 73-80.

Entenberg, D., J. Wyckoff, B. Gligorijevic, E.T. Roussos, V.V. Verkhusha, J.W. Pollard & J. Condeelis, (2011) Setup and use of a two-laser multiphoton microscope for multichannel intravital fluorescence imaging. *Nat Protoc* **6**: 1500-1520.

Farina, K.L., J.B. Wyckoff, J. Rivera, H. Lee, J.E. Segall, J.S. Condeelis & J.G. Jones, (1998) Cell motility of tumor cells visualized in living intact primary tumors using green fluorescent protein. *Cancer Res* **58**: 2528-2532.

Fidler, I.J., (1970) Metastasis: quantitative analysis of distribution and fate of tumor emboli labeled with 125 I-5-iodo-2'-deoxyuridine. *Journal of the National Cancer Institute* **45**: 773-782.

Fields, S., (2001) The interplay of biology and technology. *Proc Natl Acad Sci U S A* **98**: 10051-10054.

Fluegen, G., A. Avivar-Valderas, Y. Wang, M.R. Padgen, J.K. Williams, A.R. Nobre, V. Calvo, J.F. Cheung, J.J. Bravo-Cordero, D. Entenberg, J. Castracane, V. Verkhusha, P.J. Keely, J. Condeelis & J.A. Aguirre-Ghiso, (2017) Phenotypic heterogeneity of disseminated tumour cells is preset by primary tumour hypoxic microenvironments. *Nature cell biology* **19**: 120-132.

Forse, C.L., S. Agarwal, D. Pinnaduwage, F. Gertler, J.S. Condeelis, J. Lin, X. Xue, K. Johung, A.M. Mulligan, T.E. Rohan, S.B. Bull & I.L. Andrulis, (2015) Menacalc, a quantitative method of metastasis assessment, as a prognostic marker for axillary node-negative breast cancer. *BMC Cancer* **15**: 483.

Giampieri, S., C. Manning, S. Hooper, L. Jones, C.S. Hill & E. Sahai, (2009) Localized and reversible TGFbeta signalling switches breast cancer cells from cohesive to single cell motility. *Nature cell biology* **11**: 1287-1296.

Gligorijevic, B., A. Bergman & J. Condeelis, (2014) Multiparametric classification links tumor microenvironments with tumor cell phenotype. *PLoS Biol* **12**: e1001995.

Gligorijevic, B., D. Entenberg, D. Kedrin, J. Segall, J. van Rheenen & J. Condeelis, (2010) Intravital Imaging and Photoswitching in Tumor Invasion and Intravasation Microenvironments. *Micros Today* **18**: 34-37.

Goldstein, L.J., A. O'Neill, J.A. Sparano, E.A. Perez, L.N. Shulman, S. Martino & N.E. Davidson, (2008) Concurrent doxorubicin plus docetaxel is not more effective than concurrent doxorubicin plus cyclophosphamide in operable breast cancer with 0 to 3 positive axillary nodes: North American Breast Cancer Intergroup Trial E 2197. *J Clin Oncol* **26**: 4092-4099.

Gonzalez-Angulo, A.M., F. Morales-Vasquez & G.N. Hortobagyi, (2007) Overview of resistance to systemic therapy in patients with breast cancer. *Advances in experimental medicine and biology* **608**: 1-22.

Goppert-Mayer, M., (2009) Elementary processes with two quantum transitions. *Ann Phys-Berlin* **18**: 466-479.

Goswami, S., U. Philippar, D. Sun, A. Patsialou, J. Avraham, W. Wang, F. Di Modugno, P. Nistico, F.B. Gertler & J.S. Condeelis, (2009) Identification of invasion specific splice variants of the cytoskeletal protein Mena present in mammary tumor cells during invasion in vivo. *Clin Exp Metastasis* **26**: 153-159.

Goswami, S., E. Sahai, J.B. Wyckoff, M. Cammer, D. Cox, F.J. Pixley, E.R. Stanley, J.E. Segall & J.S. Condeelis, (2005) Macrophages promote the invasion of breast

carcinoma cells via a colony-stimulating factor-1/epidermal growth factor paracrine loop. *Cancer Res* **65**: 5278-5283.

Groenendijk, F.H. & R. Bernards, (2014) Drug resistance to targeted therapies: deja vu all over again. *Molecular oncology* **8**: 1067-1083.

Hanahan, D. & R.A. Weinberg, (2011) Hallmarks of cancer: the next generation. *Cell* **144**: 646-674.

Harney, A.S., E.N. Arwert, D. Entenberg, Y. Wang, P. Guo, B.Z. Qian, M.H. Oktay, J.W. Pollard, J.G. Jones & J.S. Condeelis, (2015) Real-Time Imaging Reveals Local, Transient Vascular Permeability, and Tumor Cell Intravasation Stimulated by TIE2hi Macrophage-Derived VEGFA. *Cancer Discovery* **5**: 932-943.

Harney, A.S., G.S. Karagiannis, J. Pignatelli, B.D. Smith, E. Kadioglu, S.C. Wise, M.M. Hood, M.D. Kaufman, C.B. Leary, W.P. Lu, G. Al-Ani, X. Chen, D. Entenberg, M.H. Oktay, Y. Wang, L. Chun, M. De Palma, J.G. Jones, D.L. Flynn & J.S. Condeelis, (2017) The Selective Tie2 Inhibitor Rebastinib Blocks Recruitment and Function of Tie2(Hi) Macrophages in Breast Cancer and Pancreatic Neuroendocrine Tumors. *Molecular Cancer Therapeutics* **16**: 2486-2501.

Harney, A.S., Y. Wang, J.S. Condeelis & D. Entenberg, (2016) Extended Time-lapse Intravital Imaging of Real-time Multicellular Dynamics in the Tumor Microenvironment. *Journal of visualized experiments : JoVE*: e54042.

Harper, K.L., M.S. Sosa, D. Entenberg, H. Hosseini, J.F. Cheung, R. Nobre, A. Avivar-Valderas, C. Nagi, N. Girnius, R.J. Davis, E.F. Farias, J. Condeelis, C.A. Klein & J.A. Aguirre-Ghiso, (2016) Mechanism of early dissemination and metastasis in Her2(+) mammary cancer. *Nature* **540**: 589-612.

Hart, I.R., (1982) 'Seed and soil' revisited: mechanisms of site-specific metastasis. *Cancer metastasis reviews* **1**: 5-16.

He, G.S., L.S. Tan, Q. Zheng & P.N. Prasad, (2008) Multiphoton absorbing materials: molecular designs, characterizations, and applications. *Chem Rev* **108**: 1245-1330.

Hoshi, A., H. Yamashita, H. Sasaki, Y. Kobayashi, M. Shima, M. Tokunaga, Y. Usui, H. Miyakita & T. Terachi, (2004) [A case of squamous metaplasia of the ureter]. *Hinyokika Kiyo* **50**: 207-209.

Hulit, J., D. Kedrin, B. Gligorijevic, D. Entenberg, J. Wyckoff, J. Condeelis & J.E. Segall, (2012) The use of fluorescent proteins for intravital imaging of cancer cell invasion. *Methods in molecular biology* **872**: 15-30.

Jayson, G.C., R. Kerbel, L.M. Ellis & A.L. Harris, (2016) Antiangiogenic therapy in oncology: current status and future directions. *Lancet* **388**: 518-529.

Joy, A.A., (2008) San Antonio Breast Cancer Symposium 2007 - Adjuvant endocrine therapy update: ATAC 100 highlights. *Curr Oncol* **15**: 68-69.

Karagiannis, G.S., J.M. Pastoriza, Y. Wang, A.S. Harney, D. Entenberg, J. Pignatelli, V.P. Sharma, E.A. Xue, E. Cheng, T.M. D'Alfonso, J.G. Jones, J. Anampa, T.E. Rohan, J.A. Sparano, J.S. Condeelis & M.H. Oktay, (2017) Neoadjuvant chemotherapy induces breast cancer metastasis through a TMEM-mediated mechanism. *Science Translational Medicine* **9**.

Katharina, P., (2011) Tumor cell seeding during surgery-possible contribution to metastasis formations. *Cancers (Basel)* **3**: 2540-2553.

Kawano, H., T. Kogure, Y. Abe, H. Mizuno & A. Miyawaki, (2008) Two-photon dual-color imaging using fluorescent proteins. *Nat Methods* **5**: 373-374.

Kedrin, D., J. Wyckoff, E. Sahai, J. Condeelis & J.E. Segall, (2007) Imaging tumor cell movement in vivo. *Curr Protoc Cell Biol* **Chapter 19**: Unit 19 17.

Kobat, D., M.E. Durst, N. Nishimura, A.W. Wong, C.B. Schaffer & C. Xu, (2009) Deep tissue multiphoton microscopy using longer wavelength excitation. *Opt Express* **17**: 13354-13364.

Kogure, T., H. Kawano, Y. Abe & A. Miyawaki, (2008) Fluorescence imaging using a fluorescent protein with a large Stokes shift. *Methods* **45**: 223-226.

Krause, M., E.W. Dent, J.E. Bear, J.J. Loureiro & F.B. Gertler, (2003) Ena/VASP proteins: regulators of the actin cytoskeleton and cell migration. *Annu Rev Cell Dev Biol* **19**: 541-564.

Kwasnitschka, T., K. Koser, J. Sticklus, M. Rothenbeck, T. Weiss, E. Wenzlaff, T. Schoening, L. Triebe, A. Steinfuhrer, C. Devey & J. Greinert, (2016) DeepSurveyCam--A Deep Ocean Optical Mapping System. *Sensors (Basel)* **16**: 164.

Lakowicz, J.R., (2006) *Principles of fluorescence spectroscopy,* p. xxvi, 954 p. Springer, New York.

Langenbeck, B., (1841) On the development of cancer in the veins, and the transmission of cancer from man to the lower animals. *English Translation, Edin Med Surg J* **55**: 251-253.

Lee, Y.T., (1983) Breast carcinoma: pattern of metastasis at autopsy. *J Surg Oncol* **23**: 175-180.

Lehmann, S., V. Te Boekhorst, J. Odenthal, R. Bianchi, S. van Helvert, K. Ikenberg, O. Ilina, S. Stoma, J. Xandry, L. Jiang, R. Grenman, M. Rudin & P. Friedl, (2017) Hypoxia Induces a HIF-1-Dependent Transition from Collective-to-Amoeboid Dissemination in Epithelial Cancer Cells. *Curr Biol* **27**: 392-400.

Levin, I. & M.J. Sittenfield, (1911) On the Mechanism of the Formation of Metastases in Malignant Tumors : An Experimental Study. *The Journal of experimental medicine* **14**: 148-158.

Lin, E.Y., J.G. Jones, P. Li, L. Zhu, K.D. Whitney, W.J. Muller & J.W. Pollard, (2003) Progression to malignancy in the polyoma middle T oncoprotein mouse breast cancer model provides a reliable model for human diseases. *The American journal of pathology* **163**: 2113-2126.

Liotta, L.A., J. Kleinerman & G.M. Saidel, (1974) Quantitative relationships of intravascular tumor cells, tumor vessels, and pulmonary metastases following tumor implantation. *Cancer Res* **34**: 997-1004.

Lobov, I.B., R.A. Renard, N. Papadopoulos, N.W. Gale, G. Thurston, G.D. Yancopoulos & S.J. Wiegand, (2007) Delta-like ligand 4 (Dll4) is induced by VEGF as a negative regulator of angiogenic sprouting. *Proc Natl Acad Sci U S A* **104**: 3219-3224.

Loo, B.W., Jr., W. Meyer-Ilse & S.S. Rothman, (2000) Automatic image acquisition, calibration and montage assembly for biological X-ray microscopy. *J Microsc* **197**: 185-201.

Masedunskas, A., N. Porat-Shliom, M. Tora, O. Milberg & R. Weigert, (2013) Intravital microscopy for imaging subcellular structures in live mice expressing fluorescent proteins. *Journal of visualized experiments : JoVE*.

Masters, B.R., (2001) History of the Optical Microscope in Cell Biology and Medicine. In: eLS. John Wiley & Sons, Ltd, pp.

Masters, B.R., (2010) The development of fluorescence microscopy. *eLS*.

McKeown, S.R., (2014) Defining normoxia, physoxia and hypoxia in tumours-implications for treatment response. *Br J Radiol* **87**: 20130676.

Nakasone, E.S., H.A. Askautrud, T. Kees, J.H. Park, V. Plaks, A.J. Ewald, M. Fein, M.G. Rasch, Y.X. Tan, J. Qiu, J. Park, P. Sinha, M.J. Bissell, E. Frengen, Z. Werb & M. Egeblad, (2012) Imaging tumor-stroma interactions during chemotherapy reveals contributions of the microenvironment to resistance. *Cancer cell* **21**: 488-503.

Narod, S.A., J. Iqbal & A.B. Miller, (2015) Why have breast cancer mortality rates declined? *Journal of Cancer Policy* **5**: 8-17.

Nifosì, R. & V. Tozzini, (2011) One-Photon and Two-Photon Excitation of Fluorescent Proteins. In: Fluorescent Proteins I. G. Jung (ed). Springer, pp. 3-40.

Noguera-Troise, I., C. Daly, N.J. Papadopoulos, S. Coetzee, P. Boland, N.W. Gale, H. Chieh Lin, G.D. Yancopoulos & G. Thurston, (2006) Blockade of Dll4 inhibits tumour growth by promoting non-productive angiogenesis. *Nature* **444**: 1032-1037.

Patsialou, A., J.J. Bravo-Cordero, Y. Wang, D. Entenberg, H. Liu, M. Clarke & J.S. Condeelis, (2013) Intravital multiphoton imaging reveals multicellular streaming as a

crucial component of in vivo cell migration in human breast tumors. *Intravital* **2**: e25294.

Patsialou, A., Y. Wang, J. Pignatelli, X. Chen, D. Entenberg, M. Oktay & J.S. Condeelis, (2015) Autocrine CSF1R signaling mediates switching between invasion and proliferation downstream of TGFbeta in claudin-low breast tumor cells. *Oncogene* **34**: 2721-2731.

Piatkevich, K.D., J. Hulit, O.M. Subach, B. Wu, A. Abdulla, J.E. Segall & V.V. Verkhusha, (2010) Monomeric red fluorescent proteins with a large Stokes shift. *Proc Natl Acad Sci U S A* **107**: 5369-5374.

Price, D.L., S.K. Chow, N.A. Maclean, H. Hakozaki, S. Peltier, M.E. Martone & M.H. Ellisman, (2006) High-resolution large-scale mosaic imaging using multiphoton microscopy to characterize transgenic mouse models of human neurological disorders. *Neuroinformatics* **4**: 65-80.

Proctor, J.W., (1976) Rat sarcoma model supports both "soil seed" and "mechanical" theories of metastatic spread. *Br J Cancer* **34**: 651-654.

Qian, B., Y. Deng, J.H. Im, R.J. Muschel, Y. Zou, J. Li, R.A. Lang & J.W. Pollard, (2009) A distinct macrophage population mediates metastatic breast cancer cell extravasation, establishment and growth. *PLoS One* **4**: e6562.

Rankin, E.B. & A.J. Giaccia, (2008) The role of hypoxia-inducible factors in tumorigenesis. *Cell death and differentiation* **15**: 678-685.

Richards, B. & E. Wolf, (1959) Electromagnetic diffraction in optical systems. II. Structure of the image field in an aplanatic system. In: Proceedings of the Royal Society of London A: Mathematical, Physical and Engineering Sciences. The Royal Society, pp. 358-379.

Robinson, B.D., G.L. Sica, Y.F. Liu, T.E. Rohan, F.B. Gertler, J.S. Condeelis & J.G. Jones, (2009) Tumor microenvironment of metastasis in human breast carcinoma: a potential prognostic marker linked to hematogenous dissemination. *Clinical Cancer Research* **15**: 2433-2441.

Rodriguez-Tirado, C., T. Kitamura, Y. Kato, J.W. Pollard, J.S. Condeelis & D. Entenberg, (2016) Long-term High-Resolution Intravital Microscopy in the Lung with a Vacuum Stabilized Imaging Window. *Journal of visualized experiments : JoVE*.

Roh-Johnson, M., J.J. Bravo-Cordero, A. Patsialou, V.P. Sharma, P. Guo, H. Liu, L. Hodgson & J. Condeelis, (2014) Macrophage contact induces RhoA GTPase signaling to trigger tumor cell intravasation. *Oncogene* **33**: 4203-4212.

Rohan, T.E., X. Xue, H.M. Lin, T.M. D'Alfonso, P.S. Ginter, M.H. Oktay, B.D. Robinson, M. Ginsberg, F.B. Gertler, A.G. Glass, J.A. Sparano, J.S. Condeelis & J.G. Jones, (2014) Tumor microenvironment of metastasis and risk of distant metastasis of breast cancer. *Journal of the National Cancer Institute* **106**.

Roussos, E.T., M. Balsamo, S.K. Alford, J.B. Wyckoff, B. Gligorijevic, Y. Wang, M. Pozzuto, R. Stobezki, S. Goswami, J.E. Segall, D.A. Lauffenburger, A.R. Bresnick, F.B. Gertler & J.S. Condeelis, (2011) Mena invasive (MenaINV) promotes multicellular streaming motility and transendothelial migration in a mouse model of breast cancer. *Journal of Cell Science* **124**: 2120-2131.

Roussos, E.T., Y. Wang, J.B. Wyckoff, R.S. Sellers, W. Wang, J. Li, J.W. Pollard, F.B. Gertler & J.S. Condeelis, (2010) Mena deficiency delays tumor progression and decreases metastasis in polyoma middle-T transgenic mouse mammary tumors. *Breast cancer research : BCR* **12**: R101.

Schneider, C.A., W.S. Rasband & K.W. Eliceiri, (2012) NIH Image to ImageJ: 25 years of image analysis. *Nat Methods* **9**: 671-675.

Seshamani, S., W. Lau & G. Hager, (2006) Real-time endoscopic mosaicking. *Med Image Comput Comput Assist Interv* **9**: 355-363.

Seyfried, T.N. & L.C. Huysentruyt, (2013) On the origin of cancer metastasis. *Crit Rev Oncog* **18**: 43-73.

Shapiro, I.M., A.W. Cheng, N.C. Flytzanis, M. Balsamo, J.S. Condeelis, M.H. Oktay, C.B. Burge & F.B. Gertler, (2011) An EMT-driven alternative splicing program occurs in human breast cancer and modulates cellular phenotype. *PLoS genetics* **7**: e1002218.

So, P.T., C.Y. Dong, B.R. Masters & K.M. Berland, (2000) Two-photon excitation fluorescence microscopy. *Annu Rev Biomed Eng* **2**: 399-429.

Sparano, J.A., R. Gray, M.H. Oktay, D. Entenberg, T. Rohan, X. Xue, M. Donovan, M. Peterson, A. Shuber, D.A. Hamilton, T. D'Alfonso, L.J. Goldstein, F. Gertler, N.E. Davidson, J. Condeelis & J. Jones, (2017) A metastasis biomarker (MetaSite Breast Score) is associated with distant recurrence in hormone receptor-positive, HER2-negative early-stage breast cancer. *Nature PJ Breast Cancer* **3**: 42.

Sparano, J.A. & L.J. Solin, (2010) Defining the clinical utility of gene expression assays in breast cancer: the intersection of science and art in clinical decision making. *J Clin Oncol* **28**: 1625-1627.

Subach, O.M., D. Entenberg, J.S. Condeelis & V.V. Verkhusha, (2012) A FRET-facilitated photoswitching using an orange fluorescent protein with the fast photoconversion kinetics. *J Am Chem Soc* **134**: 14789-14799.

Subach, O.M., G.H. Patterson, L.M. Ting, Y. Wang, J.S. Condeelis & V.V. Verkhusha, (2011) A photoswitchable orange-to-far-red fluorescent protein, PSmOrange. *Nat Methods* **8**: 771-777.

Suetsugu, A., Y. Osawa, M. Nagaki, S. Saji, H. Moriwaki, M. Bouvet & R.M. Hoffman, (2011) Imaging the recruitment of cancer-associated fibroblasts by liver-metastatic colon cancer. *J Cell Biochem* **112**: 949-953.

Swartz, M.A., N. Iida, E.W. Roberts, S. Sangaletti, M.H. Wong, F.E. Yull, L.M. Coussens & Y.A. DeClerck, (2012) Tumor microenvironment complexity: emerging roles in cancer therapy. *Cancer Res* **72**: 2473-2480.

Szulczewski, J.M., D.R. Inman, D. Entenberg, S.M. Ponik, J. Aguirre-Ghiso, J. Castracane, J. Condeelis, K.W. Eliceiri & P.J. Keely, (2016) In Vivo Visualization of Stromal Macrophages via label-free FLIM-based metabolite imaging. *Sci Rep* **6**: 25086.

Talmadge, J.E. & I.J. Fidler, (2010) AACR centennial series: the biology of cancer metastasis: historical perspective. *Cancer Res* **70**: 5649-5669.

Tillo, S.E., T.E. Hughes, N.S. Makarov, A. Rebane & M. Drobizhev, (2010) A new approach to dual-color two-photon microscopy with fluorescent proteins. *BMC Biotechnol* **10**: 6.

Vadakkan, T.J., J.C. Culver, L. Gao, T. Anhut & M.E. Dickinson, (2009) Peak multiphoton excitation of mCherry using an optical parametric oscillator (OPO). *Journal of fluorescence* **19**: 1103-1109.

van den Tweel, J.G. & C.R. Taylor, (2010) A brief history of pathology: Preface to a forthcoming series that highlights milestones in the evolution of pathology as a discipline. *Virchows Arch* **457**: 3-10.

Vinegoni, C., S. Lee, P.F. Feruglio & R. Weissleder, (2014) Advanced Motion Compensation Methods for Intravital Optical Microscopy. *IEEE J Sel Top Quantum Electron* **20**.

Wang, W., S. Goswami, K. Lapidus, A.L. Wells, J.B. Wyckoff, E. Sahai, R.H. Singer, J.E. Segall & J.S. Condeelis, (2004) Identification and testing of a gene expression signature of invasive carcinoma cells within primary mammary tumors. *Cancer Res* **64**: 8585-8594.

Wang, W., S. Goswami, E. Sahai, J.B. Wyckoff, J.E. Segall & J.S. Condeelis, (2005) Tumor cells caught in the act of invading: their strategy for enhanced cell motility. *Trends Cell Biology* **15**: 138-145.

Wang, W., J.B. Wyckoff, V.C. Frohlich, Y. Oleynikov, S. Huttelmaier, J. Zavadil, L. Cermak, E.P. Bottinger, R.H. Singer, J.G. White, J.E. Segall & J.S. Condeelis, (2002) Single cell behavior in metastatic primary mammary tumors correlated with gene expression patterns revealed by molecular profiling. *Cancer Res* **62**: 6278-6288.

Wang, Y., H. Wang, J. Li, D. Entenberg, A. Xue, W. Wang & J. Condeelis, (2016) Direct visualization of the phenotype of hypoxic tumor cells at single cell resolution in vivo using a new hypoxia probe. *Intravital* **5**: e1187803.

Williams, J.K., D. Entenberg, Y. Wang, A. Avivar-Valderas, M. Padgen, A. Clark, J.A. Aguirre-Ghiso, J. Castracane & J.S. Condeelis, (2016) Validation of a device for the active manipulation of the tumor microenvironment during intravital imaging. *Intravital* **5**: e1182271.

Wyckoff, J., B. Gligorijevic, D. Entenberg, J. Segall & J. Condeelis, (2011) High-resolution multiphoton imaging of tumors in vivo. *Cold Spring Harb Protoc* **2011**: 1167-1184.

Wyckoff, J., W. Wang, E.Y. Lin, Y. Wang, F. Pixley, E.R. Stanley, T. Graf, J.W. Pollard, J. Segall & J. Condeelis, (2004) A paracrine loop between tumor cells and macrophages is required for tumor cell migration in mammary tumors. *Cancer Res* **64**: 7022-7029.

Wyckoff, J.B., J.G. Jones, J.S. Condeelis & J.E. Segall, (2000a) A critical step in metastasis: in vivo analysis of intravasation at the primary tumor. *Cancer Res* **60**: 2504-2511.

Wyckoff, J.B., J.E. Segall & J.S. Condeelis, (2000b) The collection of the motile population of cells from a living tumor. *Cancer Res* **60**: 5401-5404.

Wyckoff, J.B., Y. Wang, E.Y. Lin, J.F. Li, S. Goswami, E.R. Stanley, J.E. Segall, J.W. Pollard & J. Condeelis, (2007) Direct visualization of macrophage-assisted tumor cell intravasation in mammary tumors. *Cancer Res* **67**: 2649-2656.

Zapata-Hommer, O. & O. Griesbeck, (2003) Efficiently folding and circularly permuted variants of the Sapphire mutant of GFP. *BMC Biotechnol* **3**: 5.

Zipfel, W.R., R.M. Williams, R. Christie, A.Y. Nikitin, B.T. Hyman & W.W. Webb, (2003a) Live tissue intrinsic emission microscopy using multiphoton-excited native fluorescence and second harmonic generation. *Proc Natl Acad Sci U S A* **100**: 7075-7080.

Zipfel, W.R., R.M. Williams & W.W. Webb, (2003b) Nonlinear magic: multiphoton microscopy in the biosciences. *Nature biotechnology* **21**: 1369-1377.

Zolla, V., I.T. Nizamutdinova, B. Scharf, C.C. Clement, D. Maejima, T. Akl, T. Nagai, P. Luciani, J.C. Leroux, C. Halin, S. Stukes, S. Tiwari, A. Casadevall, W.R. Jacobs, Jr., D. Entenberg, D.C. Zawieja, J. Condeelis, D.R. Fooksman, A.A. Gashev & L. Santambrogio, (2015) Aging-related anatomical and biochemical changes in lymphatic collectors impair lymph transport, fluid homeostasis, and pathogen clearance. *Aging cell* **14**: 582-594.